2008-2009

IARC Team Quadrotor

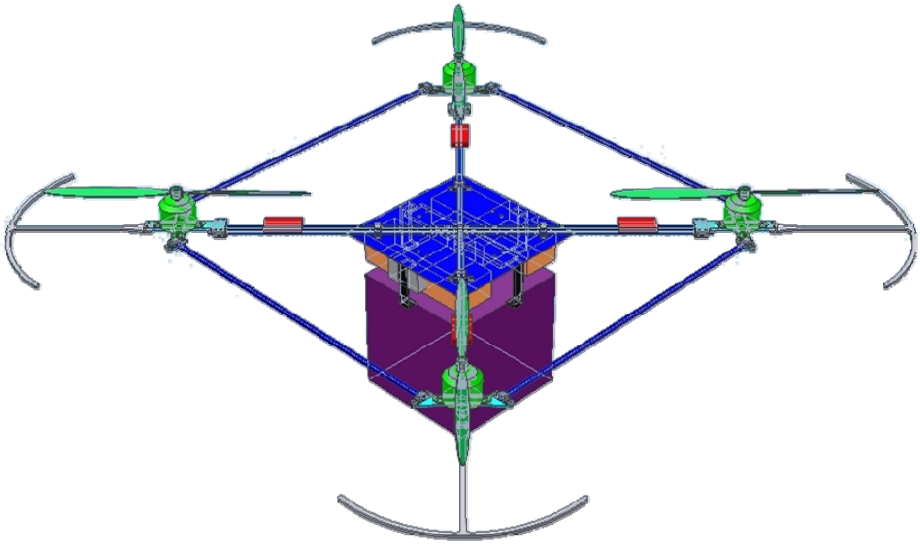

Nate Carlos

Ben Cole

John Cook

Jonathan Forest

Sansen Johnson

Ed Massie

Chris Rogers

Table of Contents

1.0 Introduction

For 2009, the International Aerial Robotics Competition will be holding its 5th mission since its inception nineteen years ago. Virginia Tech's Department of Aerospace Engineering created a team of students to compete in this year's competition. This group paired together with Mechanical Engineering students to comprise the complete Virginia Tech team that hoped to compete in the IARC competition this year. However, due to the difficulty of the design problem presented by this competition, this group will not compete in this year's IARC competition. The Mechanical Engineering students were responsible for navigation and target acquisition, which includes sensor integration and processing, while the Aerospace Engineering students were responsible for the design selection, creation, and testing of the aerial vehicle that would have been utilized in the competition. This report will cover all portions of the project up to its current state. The team identified four distinct aspects that were vital to successful completion of this year's mission. The four sub-groups of this year's IARC team were finance, propulsion, weights/structures, and flight controls. In the following sections, each sub-group will define their unique responsibilities, as well as the progress made in this academic year.

This section will cover all aspects of the competition. The competition requires that each team construct a fully autonomous aerial robot that is able to fly and navigate in a confined environment, specifically indoors. Teams are given four flight attempts. Initially, the competition vehicle (CV) will be launched from an area 3 meters away from the building. The CV will then be required to enter the target building through a one (1) square-meter opening. Once inside, the CV will have ten minutes to search, locate, and photograph a target. This information will then be transmitted back to a ground station. Obstacles such as columns, furniture, and interior walls will not be disclosed before the vehicle enters the building; thus, the CV must navigate autonomously. Upon successful completion of the mission, CV is not required to exit the building.

The target of interest will be a gauge displaying specific values. The mission is deemed a successful one if the judges are able to read a specific value on the gauge. The gauge will be surrounded by various blinking lights as well as an audible warning tone. The gauge of interest will have one non-blinking blue LED directly below it. It will be necessary for the CV to indicate that it has locked onto the target gauge by means of a JAUS-compatible message as well as a minimum of five seconds of continuous video relayed by a radio frequency. This transmission will need to have enough power to be received at one-hundred meters with a maximum loss of 6

dB. After successfully capturing the picture, the image must be relayed with enough power to be received at one-hundred meters while having a loss of only 6 dB. The receiving antenna can have an aperture no greater than one meter. In addition, the CV will be required to supply information and mission status. These include things such as navigation information, obstacle locations, as well as target location and lock status. JAUS protocol must be utilized during communication with the ground station.

The rules below are the main guidelines for the competition as they were written in the published rules [1]:

1. Vehicles must be unmanned and autonomous. They may be intelligent or preprogrammed, but they must not be flown by a remote human operator.
2. Computational power need not be carried be the air vehicle. Computers may be set up in the designated ground station area, but there can be no human intervention with any ground-based systems necessary for autonomous operation.
3. Data links will be means of radio frequencies in any legal band for the location of the arena. The vehicle must be tolerant to any and all interference that it may encounter during the mission.
4. The air vehicle(s) must be free-flying, autonomous, and have no entangling encumbrances such as tethers. During flight, the maximum dimension of the air vehicle shall not exceed one (1) meter. The maximum takeoff weight of the vehicle shall not exceed 1.50 kg. The vehicle must be powered by means of an electric motor using a battery, capacitor, or fuel cell as a source of energy.
5. Each vehicle must be equipped with a method of manual override of the propulsion system to function as flight termination. This override must be capable of operation even if all flight control system function is removed. The operation of this override will be controlled by the Judges.
6. A maximum of two (2) non-line-of-sight (NLOS) navigation aids may be used external to the designated flight area. The navigation aids must be portable, and must be removed once the team leaves the competition area. GPS, GLONASS, Galileo, or other satellite navigation systems are not allowed as navigation aids.

7. The aerial robotic system is required to be able to send vehicle status and navigation solutions of the vehicle, obstacle locations, and target location to the Judge's remote JAUS-compliant data terminal via the JAUS protocol.
8. Upon entering the arena under autonomous control, aerial robots must remain within the bounds of the arena or the attempt will end. Vehicles leaving the arena or in the Judges' opinion, are operating in an unsafe manner, will have their flight terminated by a Judge.
9. The ground station equipment and the optional navigation aids must be portable, such that it can be set up and removed with ease. All ground equipment must be able to fit through a single-wide doorway approximately 0.8 meters (32 inches) wide. Teams will not be allowed to leave behind any equipment after their flight attempt.
10. The vehicles may not drop any sub-devices in the competition arena. They may not trail any kind of tether or device to assist the air vehicle with the exception of unsupported trailing wire antennas. If the air vehicle impacts an obstacle and is able to recover without touching the ground, the attempt may continue. However, if an air vehicle lands for any reason, the attempt is over.

The competition area will have dimensions of approximately thirty meters long by fifteen meters wide, and two and a half meters high. The configuration of the interior and possible obstacles will not be disclosed before the event. It is known that control panel will not be mounted in a corridor. See Figure 1 below for an example of what the building setup could look like.

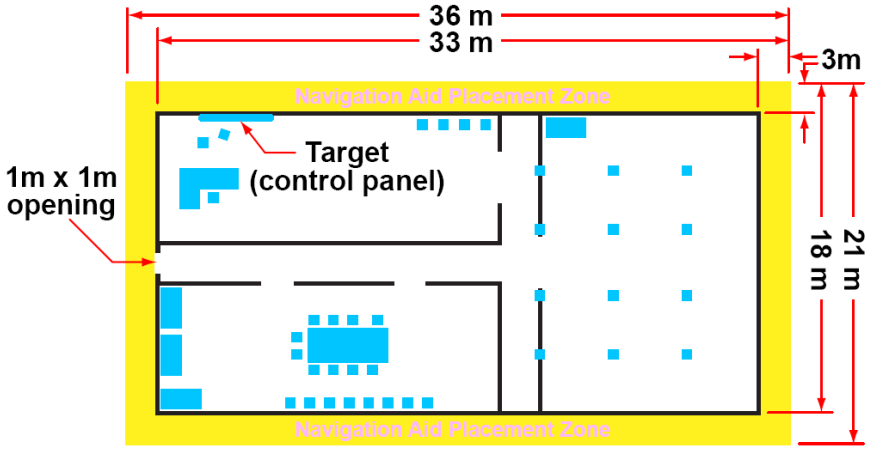

Figure 1: Example Competition Area Setup

2.0 Preliminary Design Selection

The mission objectives for this year's competition posed some interesting difficulties. The first challenge is the enclosed environment in which the vehicle will be required to operate. Given that the vehicle will spend most of its time indoors, a conventional fixed wing design did not seem appropriate given the higher forward speed required to maintain enough lift for flight. Additionally, the vehicle will be required to video and photograph a stationary position on a wall, and this favors a platform that has the ability to hover. With this in mind, the team produced a list of possible designs. The initial design concept list is below:

- Single Ducted Fan
- Single Ducted Fan with two side fans
- Dual Ducted Fan
- Lighter than Air
- Conventional Helicopter
- Coaxial Counter-Rotating Main Blade Helicopter
- Quad Rotor

The following pages will show the initial design concept sketches for each possible design case. Then, the team's design criteria will be introduced and explained. Finally, each proposed design will be analyzed, leading to the design that was selected for this year's competition.

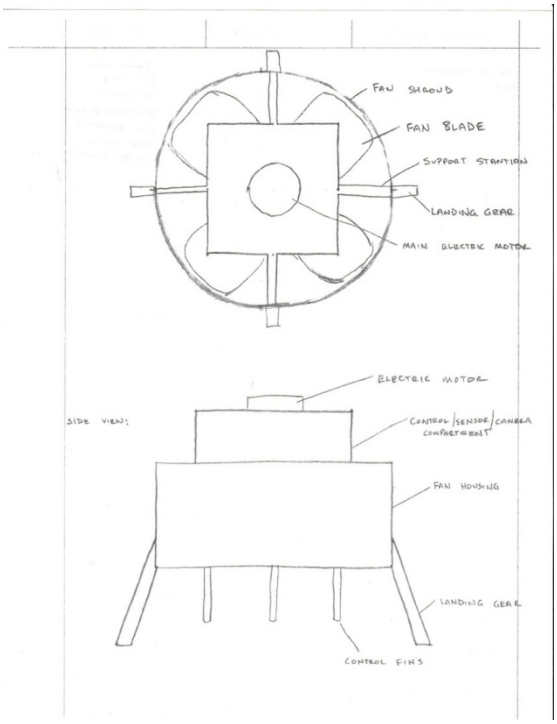

Figure 2: Single Ducted Fan

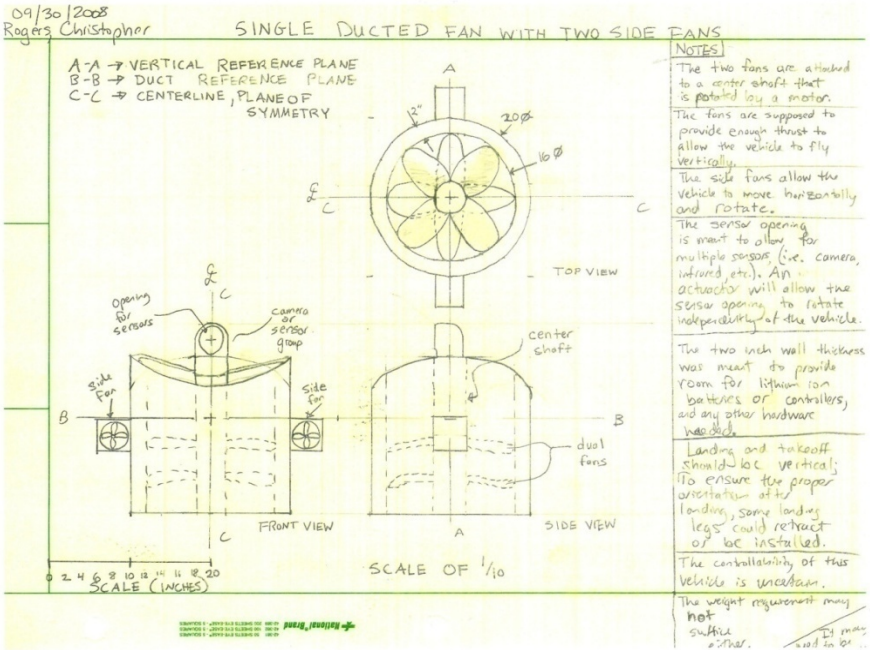

Figure 3: Single Ducted Fan with Two Fan Sides

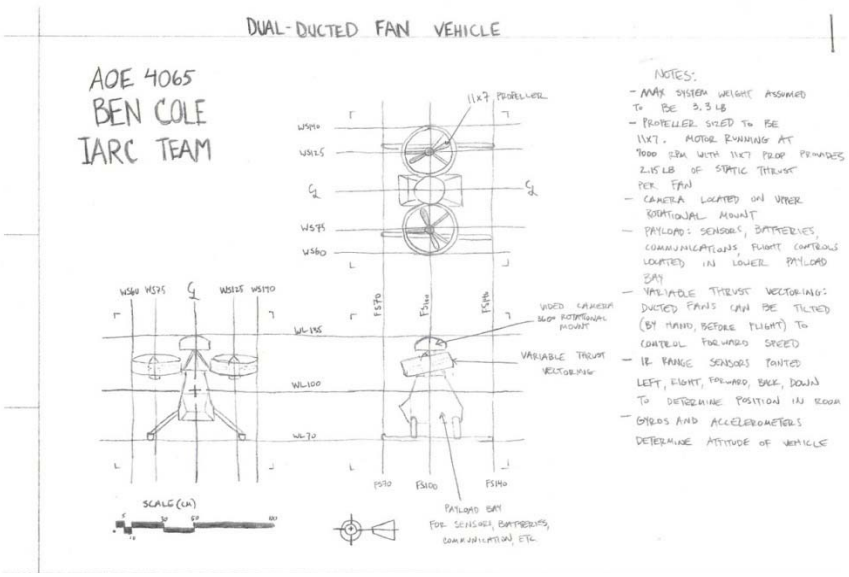

Figure 4: Dual Ducted Fan

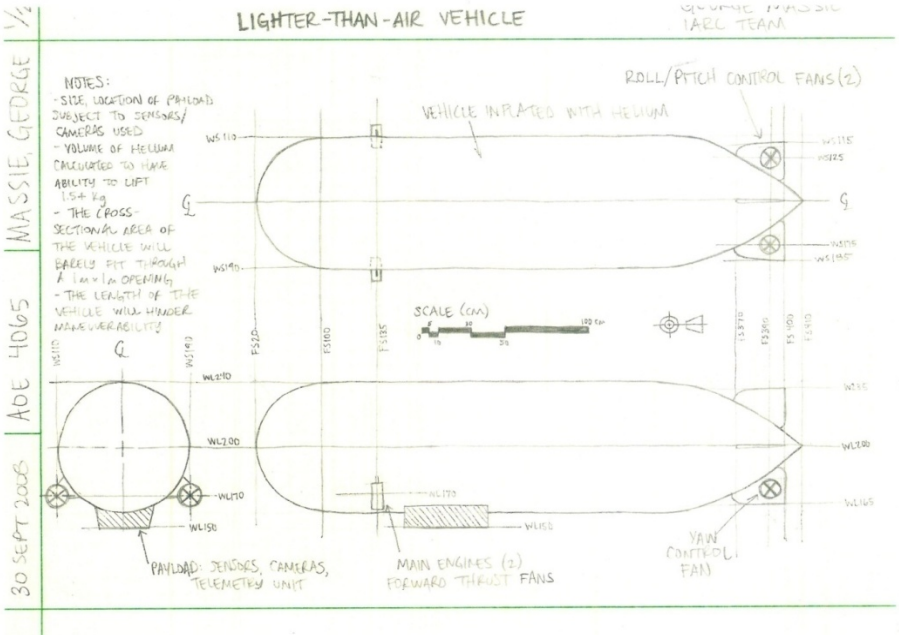

Figure 5: Lighter-Than-Air

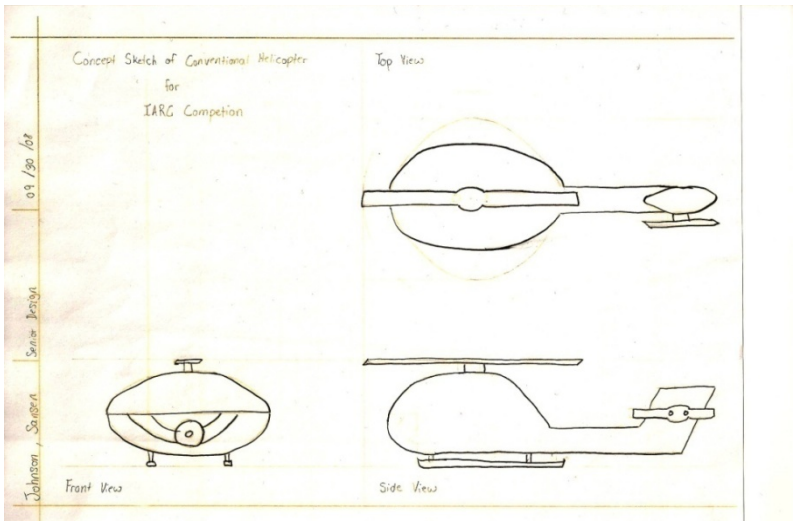

Figure 6: Conventional Helicopter

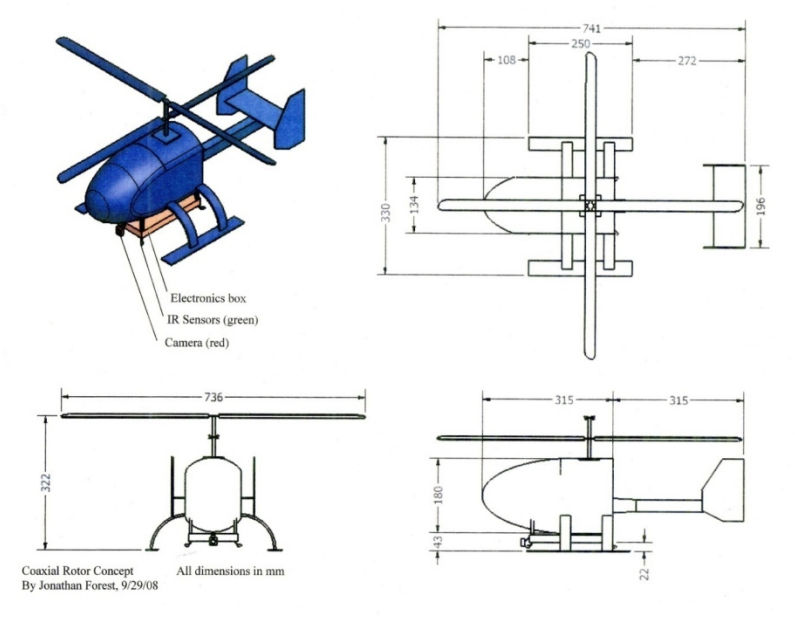

Figure 7: Coaxial Counter-Rotating Main Blade Helicopter

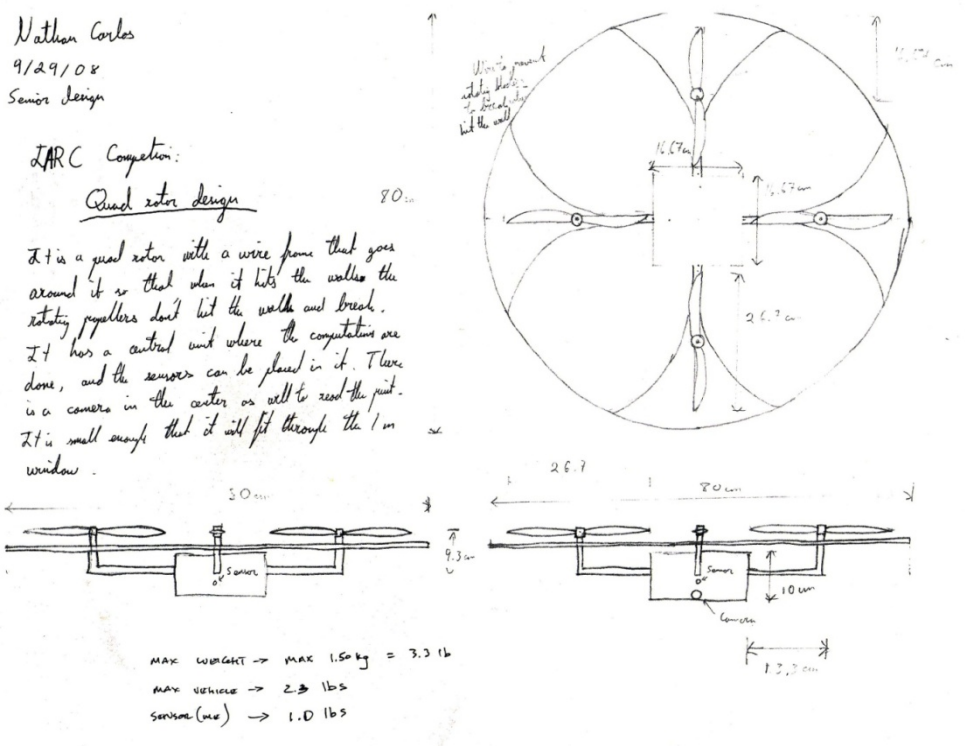

Figure 8: Quad Rotor

The team created an initial design criterion, which was established to help determine which design would accomplish the mission goals most effectively. There were six characteristics to this criterion: inherent stability assessment, controllability, useful payload, durability, vehicle gross weight, and maximum linear dimension. For ease and simplicity, a basic grading scale was created to assist the group in identifying which concept would be the best choice for the competition. There were three possible grades and respective point values that could be assigned. The first was a grade of 'undesirable' which would earn the concept a score of '-1'. The next was a grade of 'neutral' which would result in a score of '0'. Finally, was the grade of 'desirable' with a score of '1'.

The inherent stability assessment was defined as the difference between dynamic stability and dynamic instability. For this the team analyzed each case for the location of the thrust point in relation to the center of gravity. If the center of gravity was above the thrust point for the vehicle, it was defined to have an unfavorable inherent stability characteristic. An example of this was the Single Ducted Fan. For this initial design, the thrust point was considered to be the directional vanes on the very bottom of the vehicle. Given its weight distribution, the center of gravity it logically located above the thrust point giving it undesirable inherent stability with regard to accomplishing the defined mission.

Controllability was defined as the ability to easily dictate the direction of the vehicle with respect to accomplishing the IARC mission. An example of this was the Lighter than Air concept. Given that it is a tremendously stable platform, the team determined that our task of controlling its direction would be easier when compared to some of the other designs. Therefore, the Lighter than Air concept earned a grade of 'desirable' for the Controllability Design Criteria.

Useful payload was the third criteria. This was directly based on the possible vehicle's flight ready weight, as well as the possible margin of error that could be designed into the project with respect to the 1.50 kg limit. An example of this was the Lighter than Air concept. Given that its source of lift is by displacing heavier air with a relatively lighter gas, this is an extremely efficient design in terms of vehicle weight. Unfortunately, given the linear dimension restriction, the maximum allowable size was not going to be large enough to take advantage of this efficient lifting force because of the amount of weight that the vehicle would be required to lift due to the mechanical engineering package. Therefore, the Lighter than Air concept earned a grade of 'undesirable'.

The fourth criterion defined was durability. Durability is straight-forward, and was defined as the ability of the vehicle to resist damage when it came in contact with something in its surroundings. Most notorious of the group was the conventional helicopter. Given that there is no protection for the rotating main blades, the conventional helicopter earned a grade of 'undesirable'.

Gross weight was the fifth criterion. The vehicle gross weight was defined as the vehicle's flight ready weight, before any additional loads were secured. When analyzing only the vehicles weight, The Lighter than Air vehicle has the most efficient method of producing the required lift which resulted in a grade of 'desirable'.

The last criterion was maximum linear dimension. This was defined as the maximum length in any direction up to the design maximum of one meter while still being able to complete the mission objectives. An example of this was the Single Ducted Fan. Since its fan is relatively small and the sensors and controls are mounted close to the propulsion source, the overall size is not very large. This earned the Single Ducted Fan a grade of 'desirable'.

See the table below for a complete listing of each initial design concept, design criteria, and their respective scores for each category.

DESIGN CONCEPT	STABILITY	CONTROLABILITY	PAYLOAD	DURABILITY	GROSS WEIGHT	MAX DIMENSION	TOTAL
SINGLE DUCTED FAN	-1	-1	-1	1	-1	1	-2
SIDE DUCTED FAN WITH 2 SIDE FANS	-1	0	-1	1	-1	1	-1
DUAL DUCTED FAN	0	0	-1	1	-1	1	0
LIGHTER THAN AIR	1	1	-1	0	1	-1	1
CONVENTIONAL HELICOPTER	0	-1	0	-1	0	0	-2
COUNTER-ROTATING MAIN BLADE HELO	0	0	0	-1	0	0	-1
QUAD ROTOR	1	0	1	1	1	1	5

Table 1: Down Selection Matrix

3.0 Finances

For the second phase of the project, spending decreased considerably as compared to how it was when the project was first taken. This can simply be attributed to the fact that so much was learned in the development of the first prototype in phase one that development of the second prototype was more focused and purposeful. Less money was spent towards the goal of simply figuring out what works. Spending was also reigned in through the reuse of parts from Proto1 in the development of the new carbon fiber model. Another positive was the increase in financial resources, made possible by a donation of $4000 by the Virginia Center for Autonomous Systems.

A record of the team's financial activity was kept in excel sheets as before. Examples of record keeping can be found in Appendices A, B, and C. Appendix A represents a raw accountability for parts purchased, showing reference information such as part number, date of purchase, retail host, etc. Appendix B represents spending distribution across each discipline within the team, while Appendix C represents a cost analysis of the prototype as constructed.

4.0 Weights and Structures

The weights and structures subgroup was assigned with designing the overall structure of the quadrotor and keeping track of the actual and estimated weights. The overall placement and layout of components, as well as stress and deflection analysis were under the responsibility of this subgroup. In order to meet these responsibilities, the weights and structures subgroup researched and analyzed other similar quadrotor designs, analyzed various building materials and worked on building an early prototype test platform. Additionally, tables of actual and estimated weights were kept and updated as the various designs progressed.

4.1 Quadrotor Design

To meet the competition mission objectives, several design goals were set. It was decided that the quadrotor design was to have no single dimension greater than 0.8 meters in length so as to allow the vehicle to fit through the required 1 meter by 1 meter window while allowing some room for error. To meet the mission objective of having the vehicle weigh less than 1.5 kg, it was also decided to construct the quadrotor out of as many light weight materials as possible, as well as utilizing a minimal amount of structure to reduce weight and complexity. Passive stability was also of concern. To help maximize stability, it was decided to design the quadrotor in such a way as to keep the center of gravity as low as possible. Finally, the weights and structures subgroup set the goal of keeping the quadrotor design relatively simple to construct and repair. This final constraint was implemented so that as much time as possible could be devoted to testing and improving the vehicle, rather than assembling and fixing it.

In the beginning design stages, several comparable quadrotor designs were researched and analyzed. Two of the most influential designs were the BYU Quadrotor[2] and the Draganflyer X Pro[3], as seen in Figure 9.

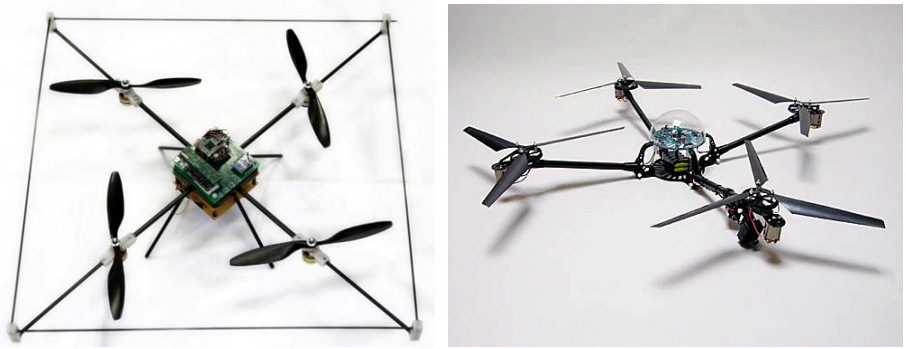

Figure 9: Design influences. At left BYU Quadrotor design[2], right photo Draganflyer X Pro [3].

The Brigham Young University (BYU) design was found to be both light weight and structurally easy to build. It had the advantage of being relatively compact, though easily accessible with many interchangeable parts. It had the positive aspect of also being built from scratch, thus giving many design ideas as to how to construct certain parts of the vehicle. Being that the BYU design lacked many features and sensors that would be needed, however, its spars and joints were designed to support less than 0.8 kg and were said to be "relatively fragile" [2] even for its own weight.

The *Draganflyer X Pro* is a well known commercial quadrotor, and was one of the earliest design examples found. While structurally sturdier than the BYU design and capable of lifting a limited payload, it was found to utilize too many specialty parts to mimic in a custom built quadrotor design. Additionally, while this design did carry several onboard accelerometers, it lacked any external sensors and provided no truly ideal locations that would provide a 360° sensor view.

As expected, there were no quadrotor designs that exactly met the specifications required by our design goals and the competition rules. Research of other designs such including those in Figure 9 did provide many design ideas of what could be possible. Work was begun on creating a viable quadrotor design using Autodesk Inventor 2009.

Autodesk Inventor 2009 was chosen as the design platform due to its robustness in design abilities. In Autodesk Inventor, one begins by modeling individual 3D parts that were to be used in the design. Once all the required parts were modeled, they were fit together in an "assembly," where constraints were applied to the movements or status of each part. From here, 2D sketches with their associated dimensions could be created of either the whole assembly (the entire quadrotor vehicle) or of each individual part (the motor spars for example). One advantage of this construction was that it allowed individual parts or dimensions to be easily changed, with the entire design and each drawing automatically being updated with the changes. Additionally, individual parts could be assigned specific materials, allowing weight estimates, moments of inertia and stresses to be easily calculated through Autodesk Inventor.

Using this program, two slightly different designs were created. The first design was designated Proto1 (short for "Prototype 1") and was intended to be a simple proof of concept model for testing, with no intention of it developing into the competition model. The second design was designated the Proto2, which was very similar to Proto1 in basic structural layout,

though it would incorporate more advanced materials and custom parts as it was intended to be the design used in competition. It was originally intended to have Proto 2 built and ready to test early enough that a second carbon fiber design could be built or updated if needed. Delays in its construction led to only one carbon fiber model being built.

4.1.1 Proto1

The design of Proto1 can be seen in Figure 10. While not designed to be used in competition, Proto1 was designed to be cheap, quick and easy to build, using mostly over-the-counter structural materials. As such, the main spars were to be made of basswood, the base plate made of maple and the ME team's sensor payload was to be represented by a wooden box filled with sand.

Proto1 was mainly to be used as a proof of concept of several ideas. It was believed that building a simpler design of the quad rotor early in the design process would allow for a better understanding of how many of the parts would fit together, as well as giving ideas on how to improve future designs. Additionally, having a cheap, quick-to-build prototype would allow for other subgroups to test their systems on a quadrotor platform similar in design and weight to what was going to be used in competition.

In Figure 10, one can see the overall layout and primary dimensions of Proto1's design. Most of the components were color coded by function or type for easy recognition. The main structure of the quad rotor was colored in shades of blue and black, and included the base plate, main motor spars, and payload connectors. The propulsion system included the motors and propellers and was colored green, while the batteries, electronic speed controllers and other associated electronic equipment was color coded in shades of orange and red. The ME payload was represented by the large purple box.

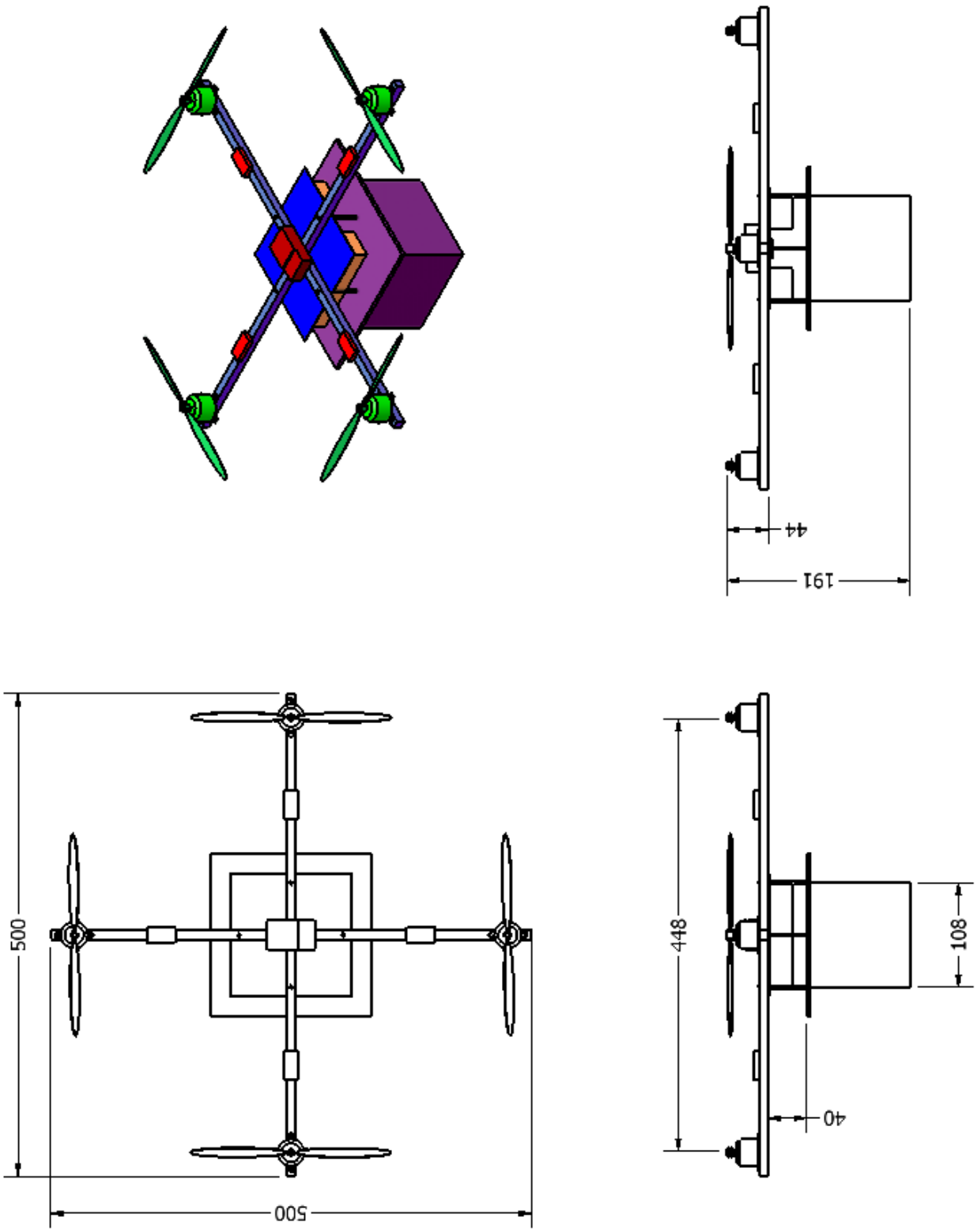

Figure 10: Proto1 design as seen in Autodesk Inventor 2009. Dimensions in millimeters.

As can be seen in Figure 10, the spar length was designed to be 500 mm (0.5 m) long, yielding a maximum width including rotating propellers of less than 700 mm (0.7 m). This spar length was determined to provide both tolerable moments on the spars and an acceptable maximum dimension, while comparative quadrotors and early propulsion interference estimates suggested this smaller spar length would not be detrimental to performance. In fact it was found that the spar length could actually be decreased without any major loss in performance.

Figure 10 displays the main spars crossing in overlap in the center of the base plate. This design feature was accomplished by notching both spars to allow them to overlay each other, while they were mounted to the quad rotor near the edge of the base plate. This configuration was chosen, as it allowed the spars to experience fewer stresses than they would under similar loading conditions had they been mounted more like cantilever beams.

Finally, the ME payload as seen in Figure 10 was placed below the main quadrotor for several reasons. This placement would be ideal in allowing the ME sensors team a full 360° view around the vehicle, while also allowing it to double as a landing pad for the vehicle. Additionally, this placement of one of the heaviest components in the vehicle would help keep the center of gravity low and assist in giving the vehicle some passive stability. While it was not planned to attach the actual ME sensor package to Proto1, a wooden box filled with sand was used to represent this payload. In this way, the overall weight of Proto1 could be adjusted for testing purposes, while still keeping the moments of inertia of the vehicle roughly the same as what would be seen in Proto2.

4.1.2 Proto2

The carbon fiber design of Proto2 can be seen in Figure 11. This design was updated numerous times from the evaluations of Proto1, and was the design planned on being used for the final IARC competition. This design called for many light weight and more expensive parts such as carbon fiber spars and base plate, while also adding a few features missing from the design of Proto1 such as the cross spars and motor shrouds. By using lighter weight and stronger materials, it was found that the structure of Proto2 would be stiffer, stronger and lighter than that of Proto1.

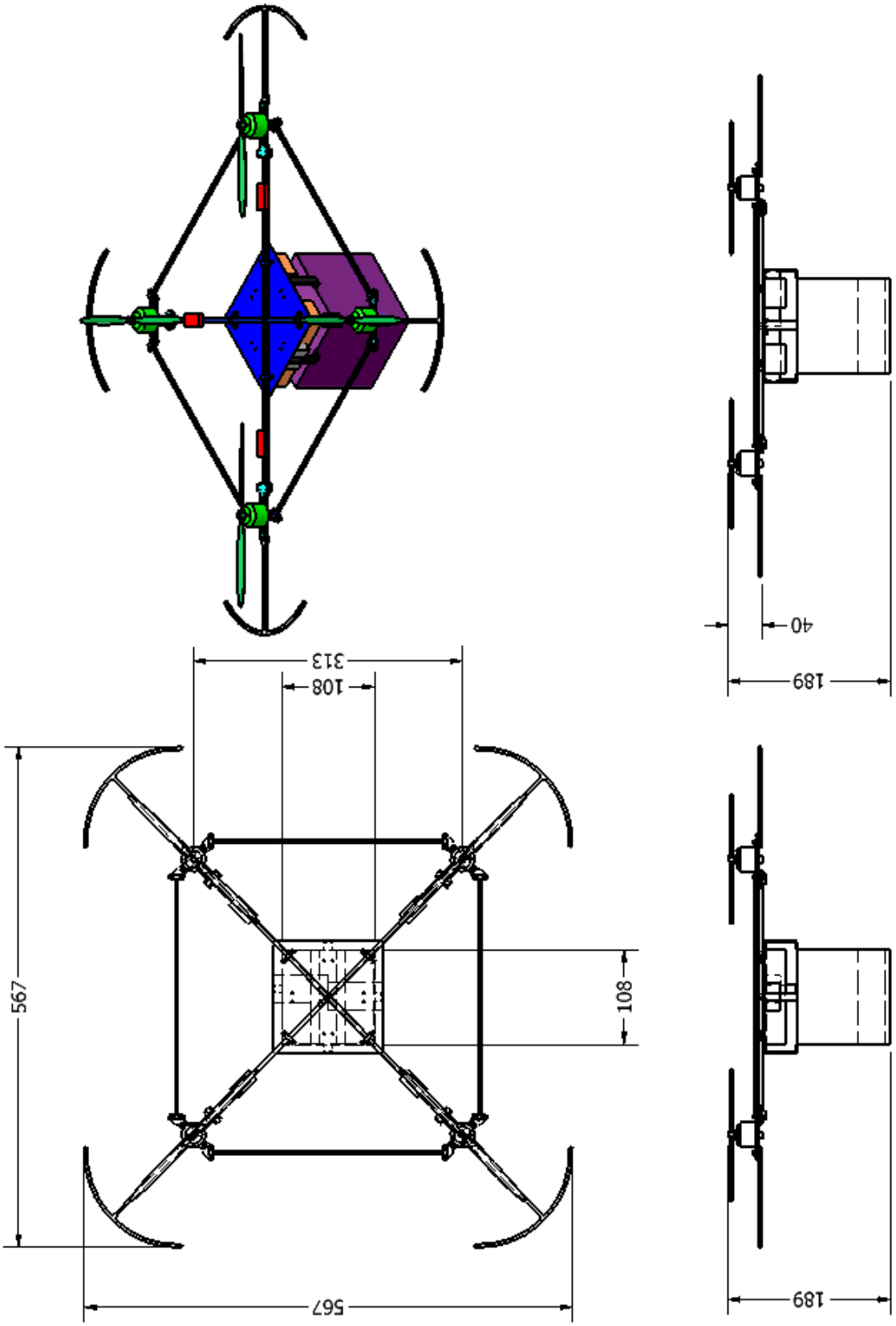

Figure 11: Proto2 as seen in Autodesk Inventor 2009. All dimensions in millimeters.

The Proto2 used the same color coding system as found in the design of Proto1 in Figure 10. From this figure, one may notice that the Proto2 design called for a few structures not seen on Proto1. The shrouds seen at the ends of the main spars had the express purpose of protecting the propeller blades from damage should the quadrotor hit a wall during autonomous flight. Additionally, one may have noticed the outer cross beam spars connected near the end of each of the main motor spars. These outer spars were implemented to reduce the twisting effects felt by the main spars while the propellers were changing speeds. It was determined that these additional spars would be necessary due to the main carbon fiber spar's smaller cross sectional area and thus reduced torsional stiffness. Additionally, it was felt that it would be beneficial from a flight control's stand point to keep the motors on a spar mount as structurally stiff as possible.

As carbon fiber was found to be much stronger than basswood, the main spars chosen for Proto2 had a much smaller cross section of 4.78 mm x 4.78 mm with an inside circular diameter of 3.05 mm (0.188 in x 0.188 in x 0.120 in). While this smaller cross section was able to save weight, it prevented the motors from being able to be attached directly onto the spars as was seen in the design of Proto1. As such, small mounts and brackets were designed and had to be custom manufactured for Proto2.

4.2 Materials

An important factor in the design of the quadrotor, both Proto1 and Proto2, were the materials used. Three primary factors were considered when choosing the materials: strength, deflection and weight. Using these criteria, several different materials were studied and compared, including aluminum 6061, G-AIMg5 fiberglass, balsa wood class IV, birch wood class IV, PVC (hard), Styrene (plastic), carbon fiber, and basswood.

Limitations of the main motor spars were the primary focus of the initial calculations, as it was determined that these parts would be experiencing the highest weights and moment out of all the parts in the quad rotor. To analyze the various materials, the bending stress and factors of safety were determined using (1) and (2) [4].

$$\sigma = \frac{My}{I_x} \tag{1}$$

Bending stress

$$FS = \frac{TensileStrength}{\sigma_{bending}} \tag{2}$$

Factor of safety formula

In addition to these variables, the beam tip displacement also played an important factor as it would affect the stability and control of the vehicle. Ideally, the designed part would experience negligible deflection under standard loadings caused by the thrust and torque produced by the motors. Initially the spars were treated as simple cantilever beams, though it was known that this estimation would actually produce results slightly worse than what would actually be experienced. Even so, it was deemed that this was an acceptable estimation as the spar mounts were attached to the base plate in such a way that lent to such estimations being accurate. The spar deflection was determined using (3) below.

$$v_{deflection} = \frac{Force \cdot Length^3}{3EI_x} \tag{3}$$

Deflection formula

Finally, weight was important because there is a 1.5 kg restriction for the competition vehicle that could not be exceeded. To calculate the weights, the density of each material was multiplied by its volume.

Figure 12 and Figure 13 were created to help analyze various materials. For simplicity, square cross sections were chosen for the analysis, though it was known that increasing the height while decreasing the width would yield improved results for all materials. In these figures, one can see that while Balsawood had the lowest weight per factor of safety, Carbon Fiber was only slightly worse. From Figure 13 one can see the relationship between deflection and weight for the various materials. In this case, carbon fiber was found to have the best ratio.

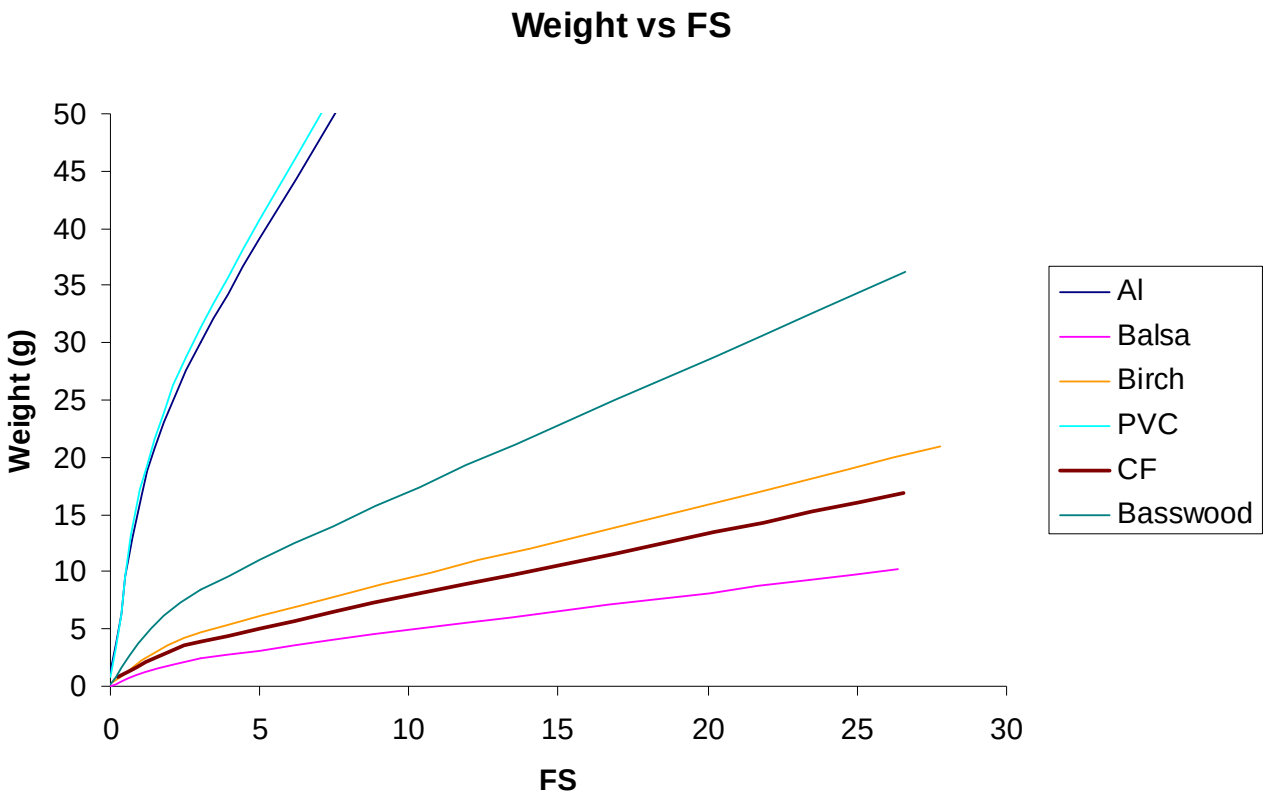

Figure 12: Weight plotted vs Factor of Safety for a square cross sectioned spar using different materials under a 1.25 lb tip load. Beam dimensions were varied and the resulting weight and FS were plotted.

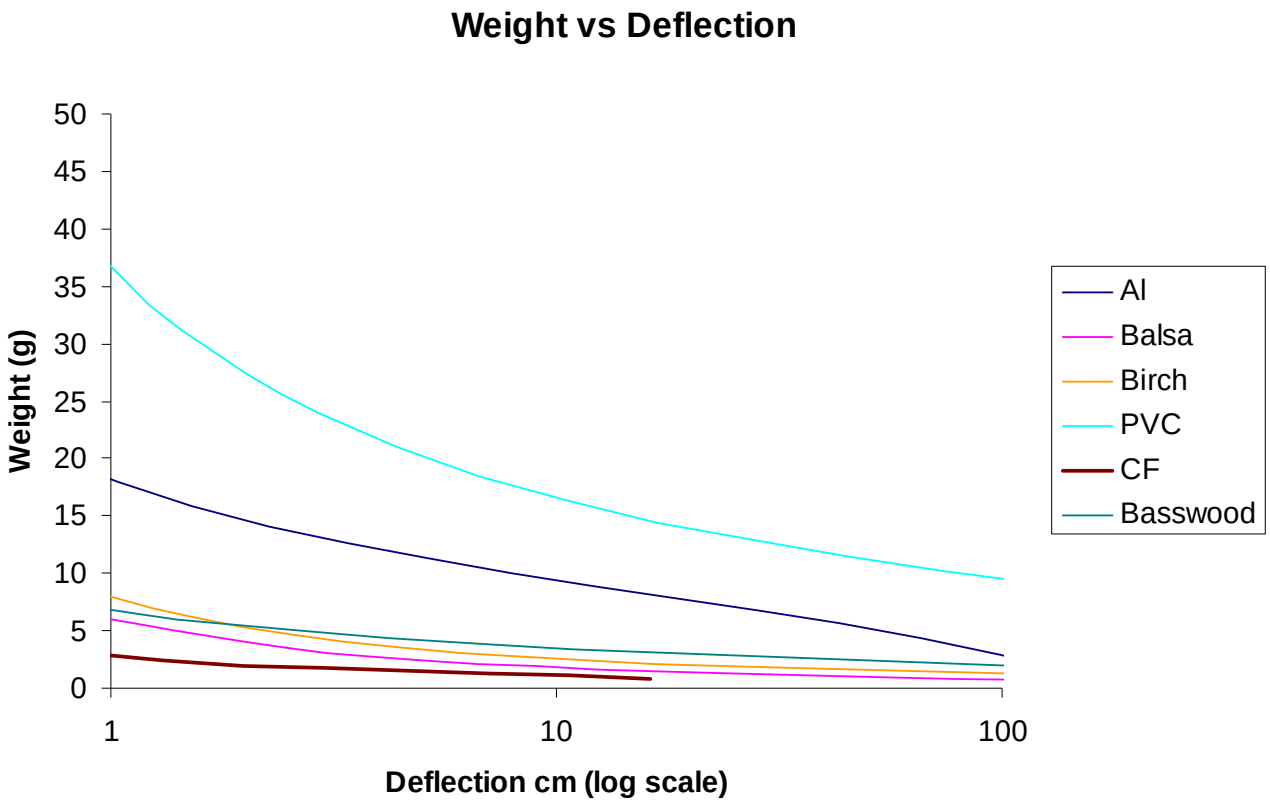

Figure 13: Weight plotted vs deflection for Safety for a square cross sectioned spar using different materials under a 1.25 lb tip load. Beam dimensions were varied and the resulting weight and deflection were plotted.

Table 2 displays the material properties, calculated deflections and factors of safeties (FS) for the various materials that were being considered. From this information, it was calculated that Balsawood Class IV would actually be the lightest material to construct the motor spars out of with carbon fiber being only a few grams heavier, though its deflection was significantly higher than that of carbon fiber. As such, carbon fiber was chosen for the spar construction material due to its low deflection rating and light weight.

Table 2: Material property calculations[5]

	Cast Aluminum G-AlMg5	Balsa Wood Class IV	Birch Wood Class IV	PVC (hard)	Styrene	Carbon Fiber	Basswood
Density (g/cm^3)	2.600	0.130	0.610	1.500	0.940	1.490	0.398
Young's Modulus E (GPa)	70.000	6.000	16.500	4.140	0.010	631.000	10.091
Tensile Strength (Gpa)	0.150	0.075	0.270	0.062	0.025	1.379	0.060
Deflection (cm)	0.275	1.272	2.553	1.431	NA	0.586	0.563
FS	3.002	3.002	3.002	3.001	3.002	3.006	3.004
b (mm)	4.810	6.060	3.954	6.456	8.740	2.297	6.525
h (mm)	4.810	6.060	3.954	6.456	8.740	2.297	6.525
Approx Weight at FS = 3	30.077	2.387	4.768	31.260	35.902	3.931	8.473

Although the calculations suggested one could build the carbon fiber spars with cross sections of less than 2.5 mm x 2.5 mm, it was decided that anything smaller than 4 mm x 4 mm (a commonly available size to purchase carbon fiber rods) would be too small to work with or mount parts to. As such, it was decided to build the spars out of 4.78 mm x 4.78 mm x 3.05 mm inner diameter carbon fiber spars (0.188 in x 0.188 in x 0.120 in ID), yielding a factor of safety of over 15, with a tip deflection of only 0.044 cm. Equivalent stresses and tip deflections for the chosen carbon fiber spar (using carbon fiber from a company called DragonPlate) were calculated using the ANYSYS finite element analysis method found in Autodesk Inventor 2009, which can be seen in Figure 14.

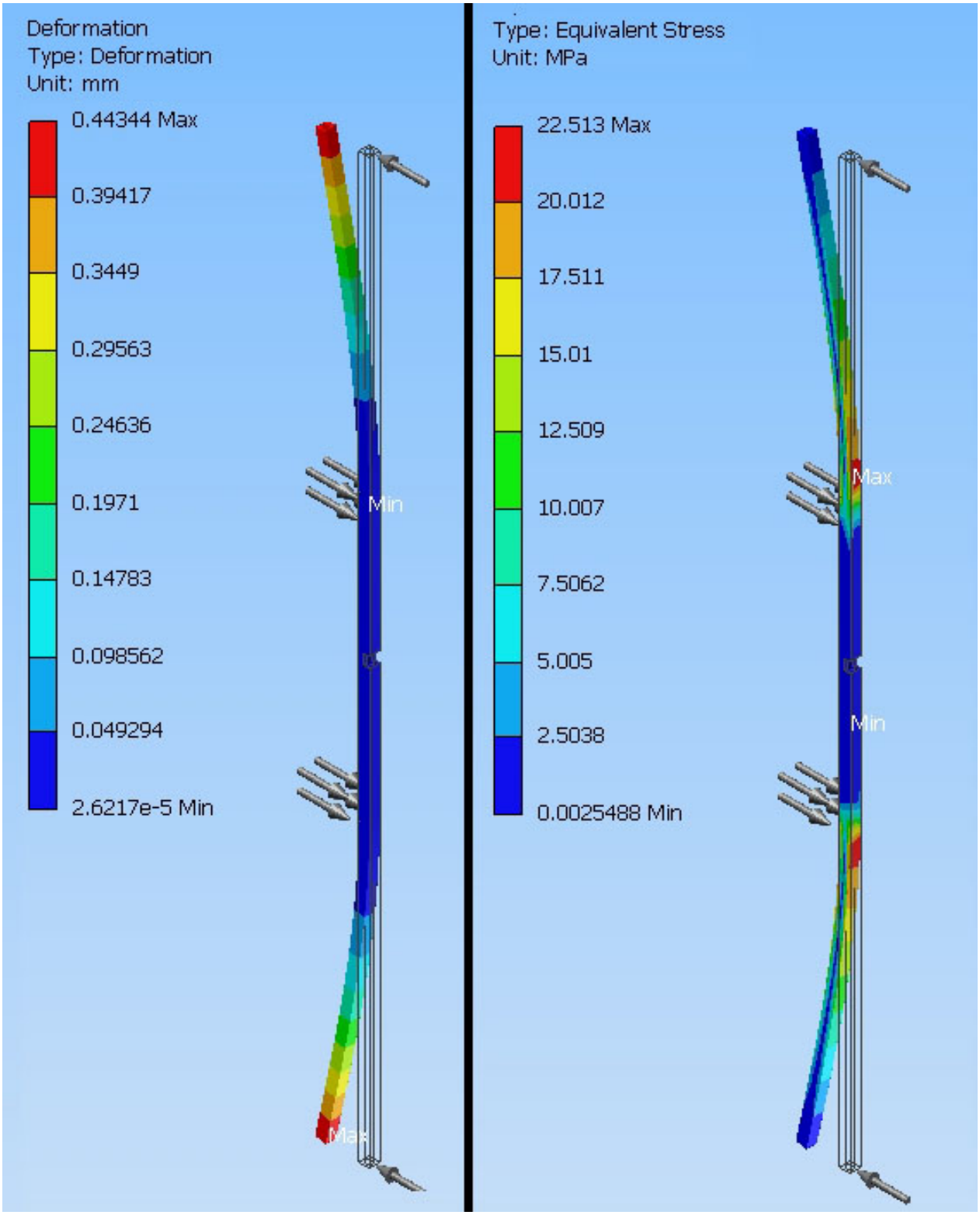

Figure 14: Deformation (left) and equivalent stress (right) analysis of carbon fiber long main spar.

For the base plate, carbon fiber was also chosen due to its favorable material properties, low weight, and strength. It was initially of concern that the carbon fiber would split after being drilled, though informal testing of a 2 mm thick carbon fiber plate yielded promising results. Assuming a worst case scenario where the vehicle was to weigh the maximum allowable value of 1.5 kg, it was calculated that the deflection of the plate would be 0.0045 cm while the factor of safety was well over 50. Again, equivalent stresses and tip deflections for the DragonPlate carbon fiber base plate were calculated using the ANYSYS finite element analysis with partial results seen in Figure 15.

Additionally, material analysis was done on the motor mounts and brackets. For these parts, aluminum 6061 was chosen due to its high strength to weight ratio and easy machinability. For these particular parts, machinability was a major concern as many high quality, high precision parts needed to be manufactured using both a CNC and milling machine. From this grouping of parts, the main motor mount plate was of the greatest concern as it would experience the most forces, it being the connecting point between the main spars, cross spars, motors and shrouds. In Figure 16 one can see some of the results from the finite element analysis. It was found that this part under maximum loading would experience a maximum deflection of 0.0157 cm, with a minimum factor of safety of 8.10.

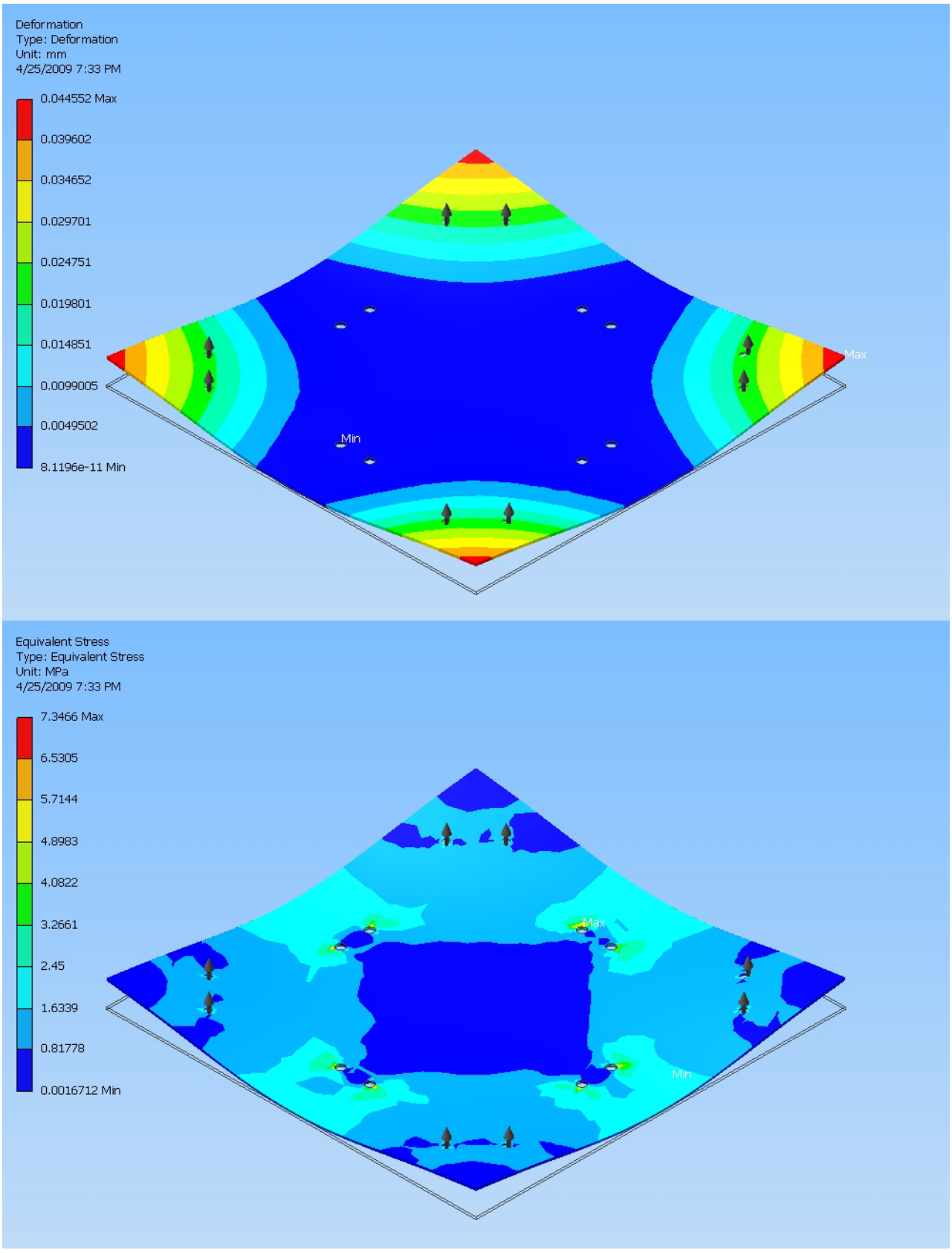

Figure 15: Deformation (top) and equivalent stress (bottom) analysis of carbon fiber base plate

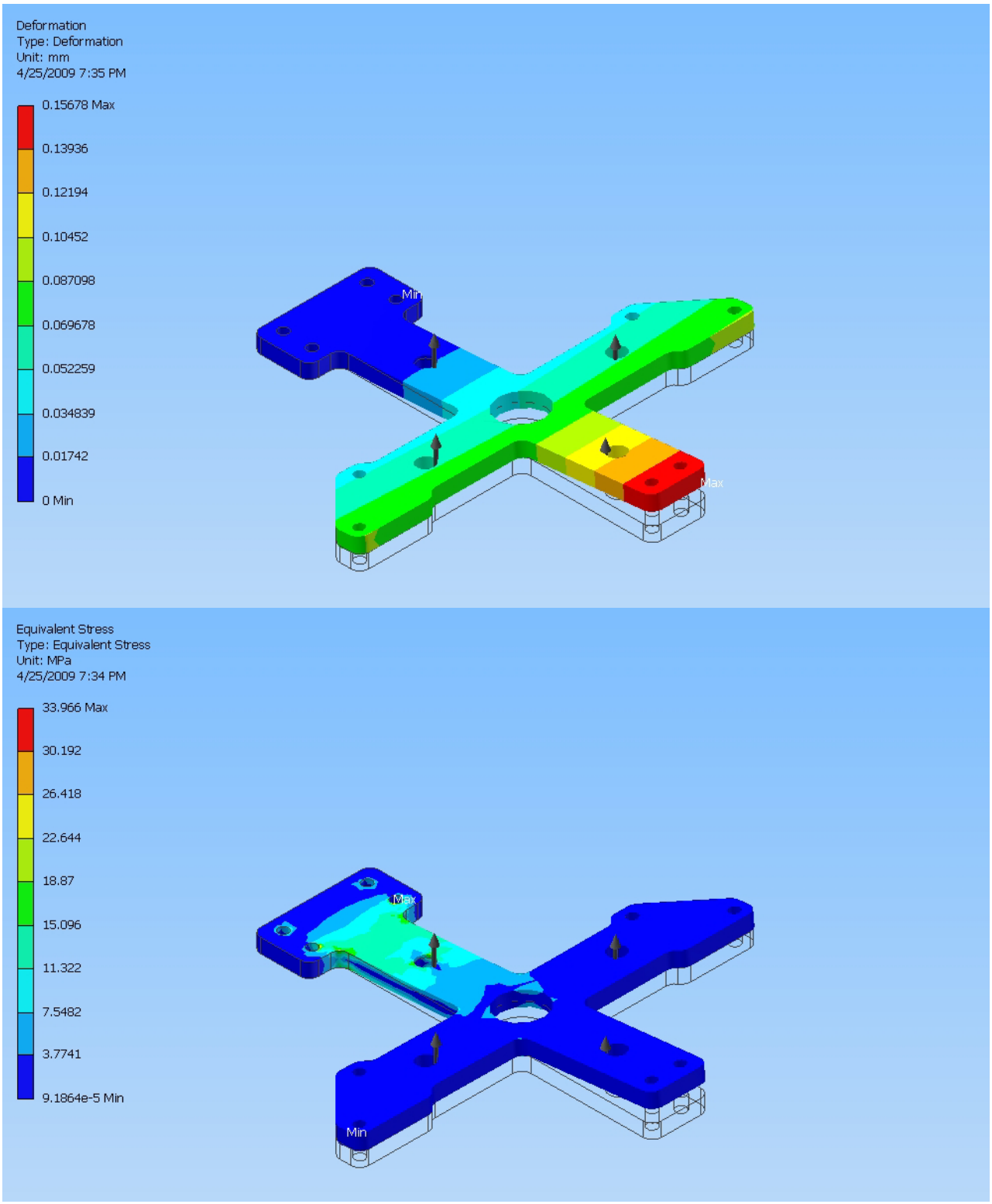

Figure 16: Deformation (top) and equivalent stress (bottom) analysis of aluminum 6061 motor mount

4.3 Proto1 Construction

Following the selection of propulsion hardware and the initial aerodynamic interference testing performed by the Propulsion Team, the first prototype was constructed. Proto1 was the first vehicle built with the purpose of serving as a method of testing propulsion and initial flight control systems.

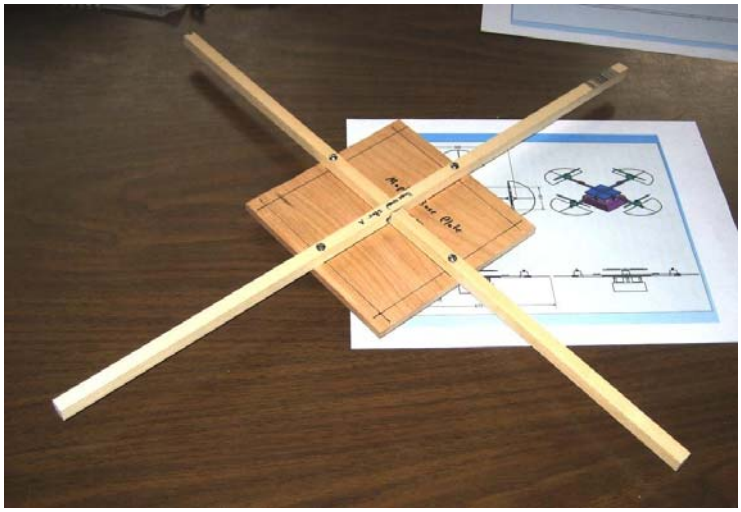

Figure 17: Maple base plate with basswood spars

The upper portion of the vehicle was constructed of 3/8 inch basswood spars, which crisscrossed and were attached to a 5.5 inch square maple base plate (Figure 17). At the end of each of the 8.5 inch arms of the vehicle, one of the Hacker A20-30M motors as seen in Section 5.3 was mounted. The motors are shipped with X-shaped mounting plates, through which two sets of bolts, nylon washers and nuts attached the motors to the spars of the craft. Each motor had an exposed section of rotating shaft which protruded from the bottom of the motor structure, which required space to spin within the spars. These extensions were shortened before the motors were mounted, which removed the need for extra holes to be drilled in the spars and allowed for shallow, partial holes to be drilled instead. This was done to preserve as much of the strength of the spars as possible. All of the holes drilled during the motor mounting process were sanded so that any loose wood was removed and would not interfere with the spinning motors.

Each of the four Phoenix-25 ESCs as discussed in Section 5.4 were attached to the spars using foam tape and zip-ties. They were placed along the spars such that the downwash created by the propellers could be used to cool the ESCs during operation. Care was taken to shorten the wire leads on the ESCs to prevent any slack in the wires that could be caught in the spinning propellers.

Holes were drilled through the Maple base plate and zip ties were used to attach the two Thunderpower 11.1V 2600 mAh batteries to the bottom side of the plate. Mounting the batteries under the thrust plane was done to lower the center of gravity of the craft and design in as much inherent stability as possible. The batteries were also mounted symmetrically on the base plate, as not to introduce any initial moments on the craft. Y-harnesses were used to allow each battery to power two motors, and placed in such a way that they could be connected at the last minute to the ESCs (Figure 18).

The same receiver used during the thrust testing was mounted in the center of the base plate, at the point where the two spars crossed. The receiver was attached using foam tape applied to the spars, and the receiver's wire antenna was wrapped around the base plate. A four-way y-harness was made so that the throttle control signal coming from the receiver could be split four ways with the same signal going to each one of the four ESCs.

Figure 18: Batteries with open connections and other wires stored below the base plate

The remaining length of wires was stored under the bass plate, between the batteries (Figure 18). With the throttle control signal split to all four ESCs, the last necessary connections to be made to complete the circuit were those between the batteries and the ESCs, which would be completed just prior to any testing.

Figure 19: Bolts connecting base plate to ballast box

Four 3 inch bolts were used to attach the upper section of the craft to the ballast (Figure 19). Ballast in the form of a box filled with sand was used on Proto1 to simulate the sensors and cameras to be used (as well as to increase the mass of the entire vehicle to the maximum competition mass of 1.5 kg). The box was constructed of Basswood, with dimensions 4 x 4 x 5.5 inches. The top of the box was another 5.5 inch square piece of Poplar wood to allow the bolts from the base plate to attach the two sections of the vehicle. Through the top of the box was drilled a 1 inch hole to allow for the addition of sand. A moveable flap of balsa wood was also attached to the top of the box, so that sand would not spill out of the box in the event of accidental inverting. After the rest of the prototype had been constructed and weighed, sand was added to the box to bring the total mass of the prototype to 1.5 kg. Nuts were fastened on either side of the top of the ballast box with ThreadLocker to ensure that no movement occurred during the testing.

The battery-ESC connections were then made and the controller employed in the thrust testing was used to send a throttle signal to the receiver. This initial signal was sent to ensure that the motors were all receiving power from the battery and the signal was effectively being split four ways to the motors. All four motors responded to the signal, and a tachometer was used to ensure that no major differences were being observed between the RPMs of the four motors. The motors were then throttled back to zero.

Figure 20: Completed Proto1 construction

The four APC 8x3.8 Slow Flyer propellers were then attached to the shafts of the motors. The propellers were arranged so that pairs of pusher and tractor propellers were across from each other (no two adjacent propellers were alike). The throttle was then increased again to check that the propellers were all spinning in their correct respective directions. Once that check was completed, construction of Proto1 was deemed complete, as shown in Figure 20.

4.4 Proto2 Construction

Proto2 construction began with the design and manufacturing of the custom aluminum 6061 parts. After consulting a mechanical engineering student at the Unmanned Systems Lab on Plantation Road, all of the custom parts had to be slightly updated so as to ensure ease of manufacturing. The first part to be made was the main motor mount, as seen in Figure 21.

It was determined that the easiest and most accurate way to construct the motor mount was to use a Tormach Personal CNC 1100. To accomplish this, a 3D *.step file of the desired part had to be imported into a program such as solid works, from where the part could be transformed into planal commands that could be read by the CNC machine. The end result was several files being created, one for each tooling bit, written in G-code, a sample of which can be seen in Figure 56 in the appendix.

Figure 21: Motor mount base created on CNC machine.

Unfortunately, after numerous delays and setbacks, the CNC machine at Plantation Road was only used to create one complete motor mount base plate. During the facing down phase for the other parts (a process during which a plate has its thickness reduced to any specified dimension), the CNC machine broke down. As such, an alternative had to be found. Eventually the Virginia Tech AOE department's machine shop was used to manufacture the remaining motor mounts and their spare replacements. It was here that the remaining motor mount base plates were created on another CNC machine, along with the brackets seen in Figure 22 that were created on a milling machine by professional machinists.

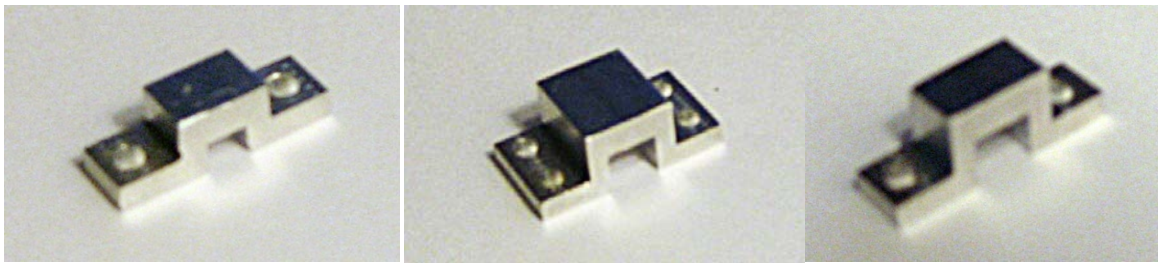

Figure 22: (left to right) Cross spar bracket, motor mount main bracket, and base plate main spar bracket, all made on a milling machine.

After manufacturing all required custom aluminum components, the ten outer perimeter holes in all four motor mount base plates had to be tapped using a #2-56 tap so that the mounting screws could be fastened directly to this base plate without the use of washers or screws, thus saving weight. Special care had to be taken so that the tap, which was much smaller than normal,

did not break off in the component. Despite this extra care however, metal shavings did at one point become wedged in the threading, breaking one of the purchased taps.

Next, the carbon fiber parts were prepared to cut and drill to specifications. As carbon fiber dust is extremely dangerous if inhaled, special safety precautions had to be taken while cutting the carbon fiber, including using medical quality respirator masks, eye protection and a shop vacuum to suction away the excess carbon fiber dust. Additionally, as carbon fiber is extremely tough, a Dremel with a special reinforced cut off wheel was used, spinning at high speed. While the reinforced cut off wheels had to be replaced regularly while cutting the carbon fiber, they had the advantage of making smooth cuts with few frays and a lessened amount of dangerous carbon fiber dust as the Dremel would actually sear the ends of the carbon fiber strands. In addition to this quality, the carbon fiber was wrapped in masking tape so as to prevent fiber fraying while it was being cut.

After the carbon fiber was cut and drilled to the specified design, the carbon fiber pieces and custom aluminum components could all be joined together by simply using pressure fittings. To connect the aluminum pieces together in such a clamp like fitting, forty-eight #2-56 screws (5/8 inches long) were used. #2 screws were chosen for these connections over the more commonly used #6 screws (which were used in mounting the motors to the quad rotor) due to their much smaller size and weight. The final result of Proto2's frame can be seen in Figure 23.

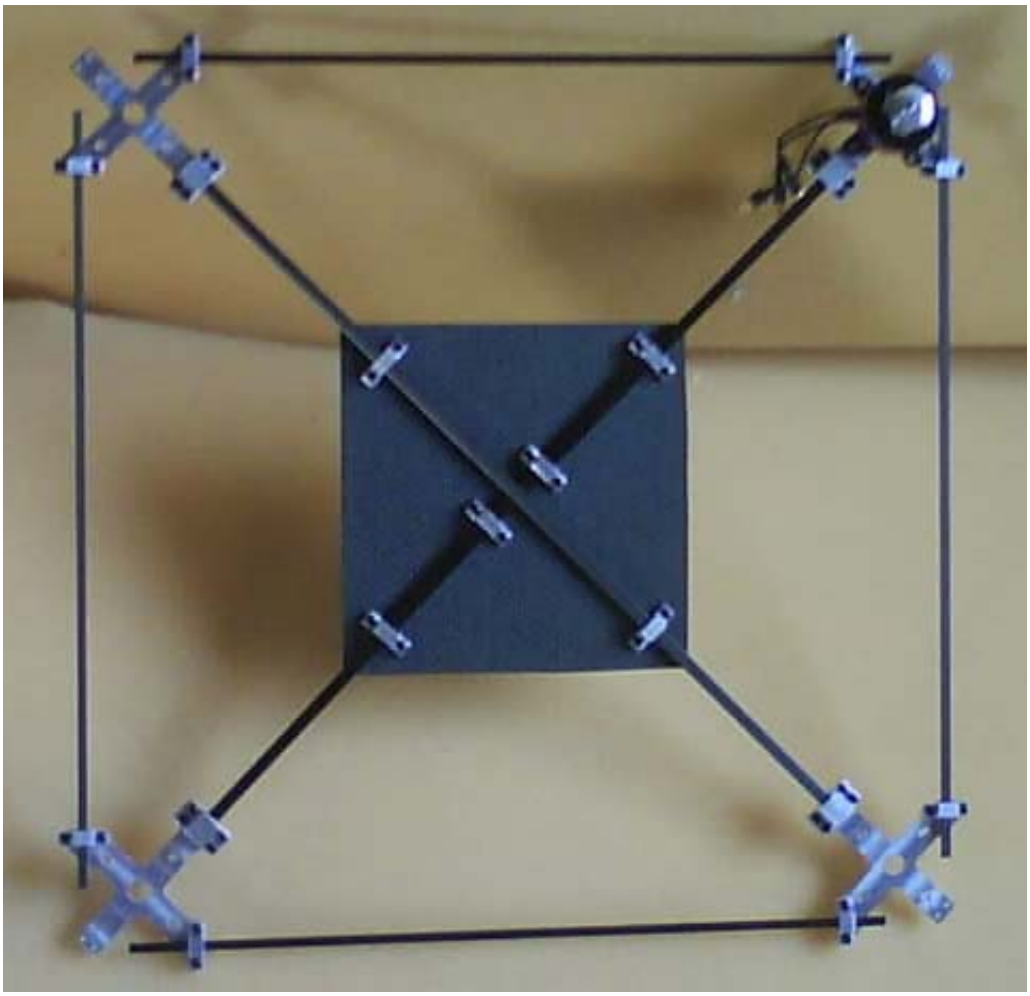

Figure 23: Proto2 frame. Note the motor in upper right mount for sizing purposes.

The next step in completing Proto2 would be to attach all the motors, electronic speed controllers, batteries and other electronics to the Proto2 frame, though at the time of this paper these materials were still being used on Proto1 for testing. It is of note, however, that this final bit of assembly should take very little time, as the hard points have already been created, needing only a few screws and zip ties to attach the final components.

Finally, it was planned to create Proto2's four shrouds seen in Figure 10 to help protect the propellers from wall collisions. Several ideas for these shrouds were considered, including aluminum 6061 machined parts, carbon fiber moldings, carbon fiber plating and nickel-aluminum wiring. The aluminum and nickel-aluminum ideas were initially rejected in favor of the lighter carbon fiber options. Several attempts at fabricating the carbon fiber parts, however, proved to be too imprecise with noticeable defects and too difficult to manufacture. As such, the machined

aluminum and nickel-aluminum wiring ideas were revisited. It was quickly discovered that the nickel-aluminum wiring option would weigh up to 60 grams to provide adequate bumper protection, resulting in the decision to fabricate the shrouds out of aluminum 6061 through the AOE machine shop. While the shrouds have not yet been completed at the time of this paper, work on them has already begun with expectations to finish their fabrication soon.

4.5 Weights

Two separate weight tables were used to keep track of each design's estimated or actual weight. When actual part weights were not available, the parts size and density were used to calculate estimates of the part's weight. It was hoped that by keeping a detailed weight table weight problems could be predicted in their early stages, while specific systems areas could be targeted for weight optimization.

4.5.1 Proto1

Table 3: Proto1 weight table

Component	Weight (g)	Qty	Total Weight (g)
Base Plate	86.7	1	86.7
Motor Spar	38.8	2	77.6
Structural Bolts	1.2	4	4.8
Washers	0.4	4	1.6
Nuts	0.0	4	0.1
Motor Mount Bolt	0.9	8	7.2
Motor Mount Nut	0.4	8	3.3
Motor Mount Washer	0.0	8	0.1
Battery Y Harness	16.2	2	32.4
ESC	17.4	4	69.7
Motor	53.7	4	214.8
Propeller	7.3	4	29
ESC Y Harness	21.4	1	21.4
Battery	185.5	2	371
Receiver	40.3	1	40.3
Zip Ties	1	4	4
		Sub Total	963.9
ME Payload Box	219.5	1	219.5
Ballast Sand	320.7	1	316.6
		Total	1500

Table 3 is a listing of actual weights that were measured for the Proto1 design. From this listing, it was verified that the major structural components that needed to be reduced in weight were the base plate and motor spars. Proto1's design was found to have a vehicle weight of 963.9

grams. While the ME sensors team had stated that their payload would weigh less than 1 pound (453.4 grams), the payload was increased in the prototype to 536.1 grams to bring the vehicle's weight to the maximum competition allowance of 1500 grams. This weight addition was implemented so that Proto1 could be tested under the maximum allowable weight, though this could be altered by removing some ballast sand. It was estimated that if the ME sensors team were to keep their payload to their estimate of 453.4 grams, Proto1's overall vehicle weight including payload would be only 1417.3 grams, thus achieving the mission's weight constraints.

4.5.2 Proto2

Table 4: Proto2 weight table

Component	Weight (g)	Qty	Total Weight
Base Plate	33.50	1	33.5
Long main spar	7.20	1	7.2
Short main spar	3.50	2	7
Cross spar	3.45	4	13.8
Motor mount	8.00	4	32
M. Mount main bracket	1.63	4	6.5
Main spar bracket	0.85	6	5.1
Cross bracket	0.65	8	5.2
#2, 5/6" screws	0.27	44	11.8
#2 washers & nylon nuts	0.21	12	2.5
Shrouds	*8.50*	*4*	*34*
#6, 3/8" screw	0.90	16	14.4
#6 washers & nuts	0.41	16	6.56
Battery Y Harness	16.20	2	32.4
ESC	17.40	4	69.6
Motor	53.70	4	214.8
Propeller	7.30	4	29.2
ESC Y Harness	21.40	1	21.4
Battery	185.50	2	371
Zip Ties	1.00	4	4
		SubTotal	921.96
ME Payload	453.6	1	453.6
		Total	1375.56
		LIMIT	1500

Table 4 is a listing of actual and estimated weights for the Proto2 design. In this table, the weight estimate for the propeller shrouds are denoted by italicized entries, while actual known weights are in normal font. From this table it was noted that even with the addition of several structural parts, the use of light weight materials brought the actual vehicle weight in at 922 grams, 42 grams less than what was seen in Proto1. This reduction in vehicle weight brought the overall estimated vehicle with payload weight to 1375.6 grams, 124.4 grams under the competition weight limit. While it was hoped to keep the vehicle as light as possible for

maximum performance, this lighter weight estimate would allow for some minor weight creep for sensors or other needed items if necessary.

5.0 Propulsion

5.1 Introduction and Design Requirements:

The propulsion subgroup was tasked with investigating and testing motors, batteries, electronic speed controllers (ESCs), and propellers with the intent to satisfy a given set of propulsion requirements. Before any hardware was investigated, the following propulsion requirements were set:

- The combined thrust requirement between four motors was set to a scale reading of 2.25 kg. Since the maximum allowable vehicle weight was 1.5 kg, thrust required to hover corresponded to a scale reading of 0.375 kg. A conservative estimate of 1.5 times the hover thrust (0.570 kg per motor) was set with the assumption that this would be sufficient for attitude adjustment and maneuvering.
- The flight endurance objective was set to greater than 10 minutes. Competition rules limit time inside the building to 10 minutes; therefore additional time was built in to the requirement to allow for time to get inside the building.
- The maximum propeller diameter was set at 9 inches. This was set to keep the overall dimensions of the vehicle within reason. Four propellers with a diameter of greater than 9 inches yields a vehicle which approaches the upper size limits for fitting through the 1 meter by 1 meter window.
- Motor Requirements:
    - To keep the vehicle mass below threshold it was determined that the mass of a single motor could not exceed 50g (excluding wires and connectors).
    - The maximum amperage draw was set at a value of 10 amps (A). The amp draw directly determines flight time and battery size; therefore a maximum amp draw of 10A should yield flight times of greater than 10 minutes.
    - The Revolutions Per Minute (RPM) of the motor was set at a minimum of 10000 RPM. This value was set by the thrust equation, which will be discussed in Section 2.0.
    - It was desired that the motor have the highest possible kV value. The kV value is a manufacturer specified constant determined by the ratio of RPM to battery voltage. Higher kV values yield higher RPM and result in greater thrust.

- The maximum operating temperature of the motors was set at 150°F, as specified by the manufactures.

- ESC Requirements:
  - The ESCs had to be lightweight, so the maximum mass was set at 30g each.
  - Programmable battery voltage cutoffs needed to be included with each ESC for battery/vehicle safety.
  - Each ESC must have a high enough current rating to endure any motor current draw.
- Battery Requirements:
  - A high energy density to weight ratio was desired for all batteries.
  - The batteries had to have the capacity to operate multiple motors for greater than 10 minutes, with a high discharge rating to allow multiple motors to simultaneously draw from each battery.
- Propeller Requirements:
  - The propellers had to be lightweight, with weights less than 10g each.
  - The maximum diameter was set at 9 inches and the pitch length limited to 8 inches.
  - Thrust requirements needed to be satisfied without fluttering or approaching manufacturer specified RPM limits.

5.2 Hardware Selection

With the above requirements outlined, motors, batteries, ESCs, and propellers were researched and tested. The motor and propeller components were chosen based on Equation 4:

$$Thurst\ (kg) = P(in) * D(in)^3 * RPM^2 * 10^{-10} * 0.02835 \quad (4)$$

General thrust equation for propellers

where *P* is the pitch length of the propeller, *D* is the diameter of the propeller, and *RPM* is the revolutions per minute of the propeller [6]. The constants on the end of (4) simply convert the number into the desired units. After choosing a variety of motors, propellers with certain pitch length and diameters were chosen so that they provide the thrust in the range of the requirements.

5.3 Motor Selection

Three classes of motors were investigated: brushless outrunner, brushed and brushless inrunner motors. A brushless outrunner motor has a stationary core and windings. The outer

shell has magnets on it and is free to rotate. The electronic speed controller creates a coil switching sequence that results in a rotating magnetic field. With the attraction of the field and the magnets on the outer shell, the shell rotates. Since the only contact points are the shaft in the bearings, these motors are extremely efficient (up to 90% in some cases) and create high torque. These motors are perfect for a direct-drive propeller setup.

Brushed motors operate in a similar manner except the inner core rotates with respect to the outer shell. With these motors, the inner shaft is in contact with commutators. These motors are inherently less efficient due to friction and provide less torque than a brushless outrunner.

Inrunner motors operate similar to brushed motors. They still have a rotating inner core, but it is held in place with a magnetic field. These motors are more efficient than a brushless outrunner and operate at extremely high RPM but create little torque. Inrunners are generally used to operate small propellers at high rates of speed or used in a geared propeller system.

5.3.1 Brushless Outrunner Motor Selection

Three Hacker motors were chosen with these being the A10-9L [7], A20-34S, and the A20-30M [8]. The motor constants and specifications are given in Table 5:

Table 5 : Motor characteristic for the three Hacker brushless outrunner motors

Motor	Weight (g)	kV (RPM/V)	Operating Amps (A)	Peak Amps (A)
A10-9L	20	1700	5	7
A20-34S	29	1500	7	10
A20-30M	42	983	11	20

Three distinct motor sizes (shown in Figure 24) were chosen to allow for a wide range of motor comparisons.

Figure 24 : From left to right: Hacker A20-30M, Hacker A20-24S, Hacker A10-9L

5.3.2 Brushed Motor Selection

Based on thorough research, it was determined that a brushless outrunner was better than a brushed motor in all aspects other than cost. With a significant budget, it was determined that brushed motors could be revisited should the need arise; however no brushed motors were initially purchased.

5.3.3 Inrunner Motor Selection

A Feigao 1208425 motor was chosen as an inrunner motor due to its low weight and high kV value of 5800 RPM/V. This motor was used to investigate a direct drive propeller system. A HiMax 2015-3666 geared inrunner was also chosen to investigate the effects of using a geared inrunner propulsion system. This setup utilized a 3600 kV inrunner motor with gearing possibilities of 4.4:1, 5.3:1, and 6.6:1.

5.4 Electronic Speed Controller Selection

The Castle Creations Phoenix-10 Electronic Speed Controller was initially chosen as the optimal ESC for the project. It was chosen for because it was lightweight, had programmable functions, and had a sufficient amperage rating [9]. However, after a failure of the ESC (discussed in Section 5.7.5) and after talking with knowledgeable individuals in the field of radio controlled models, it was decided to move up to the next largest size ESC, the Phoenix-25 [10]. Specifications on both speed controllers are listed in Table 6.

Table 6 : Electronic speed controller characteristic comparison

ESC	Weight (g)	Continuous Rating (A)	Peak Rating (A)	Programmable
Phoenix-10	6	10	15	Yes
Phoenix-25	17	25	30	Yes

5.5 Battery Selection

A Thunderpower 7.4V Prolite 2100 mAh Lithium-Polymer (LiPo) battery was chosen initially, with a mass of 100.3g. Lithium-Polymer batteries are the newest generation of batteries and as such they have the largest energy density to weight ratio [11]. This particular battery was suggested to the team by individuals on the Mechanical Engineering side of the project. The voltage of the battery and the current are independent factors. The higher the voltage of the battery, the faster the motor can spin. The higher the battery capacity (measured in mAh), the longer the runtime of the motor. Initial tests were performed and it was determined that a higher voltage battery was necessary to obtain the performance results necessary (discussed further in Section 5.7). A Thunderpower 11.1V Prolite V2 2600 mAh battery was chosen for the second iteration of batteries, with a mass 185.5g.

5.6 Propeller Selection

A wide variety of propellers were tested. The denotation for propellers is of the format *"diameter x pitch"*. The propellers tested were 9 inches in diameter or less. The pitch lengths of the propellers ranged from 3.8 inches to 8 inches. The pitch length is the distance the propeller

would move forward through the air (like a screw) in one complete revolution. The lower the pitch length, the flatter the camber of the blade.

Both helicopter rotors and aircraft propellers were tested. The helicopter rotors were chosen due to the fact that the quadrotor operates much like a helicopter and the blades experience no free stream flow. The rotors tested were manufactured by Walkera and XUFO. The propellers tested were manufactured by APC, Dragonfly, Great Planes, GWS, and Master Airscrew. The propellers and their corresponding masses are listed in Table 7. All of the propellers are tractor propellers unless otherwise denoted by "P" for pusher.

Table 7 : Summary of all propellers tested and their masses

Propeller	Weight (g)		Propeller	Weight (g)
APC 4.5x4.1 TE	3.6		APC 8x6 TE	12.5
APC 4.75x4.75 TE	3.3		Master 8x6 TRI	14.5
APC 5.5x4.5 TE	4.2		APC 8x8 TE	12.5
APC 5x5 TE	3.5		APC 9x4 REG	22.6
APC 6x4 TE	4.6		APC 9x6 TE	17.8
Master 6x4 TRI	6.7		APC 11x8 TE	21.2
APC 7.8x6 CF	14.1		XUFO-1 Rotor	5.6
Master 7x4 TRI	10.8		Dragonfly 8x4.5	5.6
APC 7x5 TE	8.1		Dragonfly 8x4.5 P	5.5
APC 8x3.8 SF	7.4		Great Planes 8x4	5.3
APC 8x3.8 SF P	7.1		Great Planes 8x6 SF	6.3
APC 8x4 REG	16.6		GWS 6x3 EP6030	2.1
APC 8x4 SRT	16.7		Master 8x4	10.2
APC 8x4 TE	12.6		Walkera 7.5 Rotor	4.3
LEGEND:				
TE: Thin Electric			SF: Slow Flyer	
REG: Regular			P: Pusher	
TRI: Tri Blade			SRT: Sport	
CF: Carbon Fiber			Final Chosen Prop:	

5.7 Thrust Testing

5.7.1 Thrust Fixture

Thrust testing was performed to characterize different combinations of motors and propellers as viable options for the vehicle. To perform the tests, a stand needed to be constructed that would effectively display the equivalent mass that could be levitated by each motor/propeller combination.

The Virginia Tech Design-Build-Fly team was consulted, because of their experience with propeller-driven aircraft. The team did have a thrust test apparatus; however it was in need of repair and it was decided that the IARC team would build one instead.

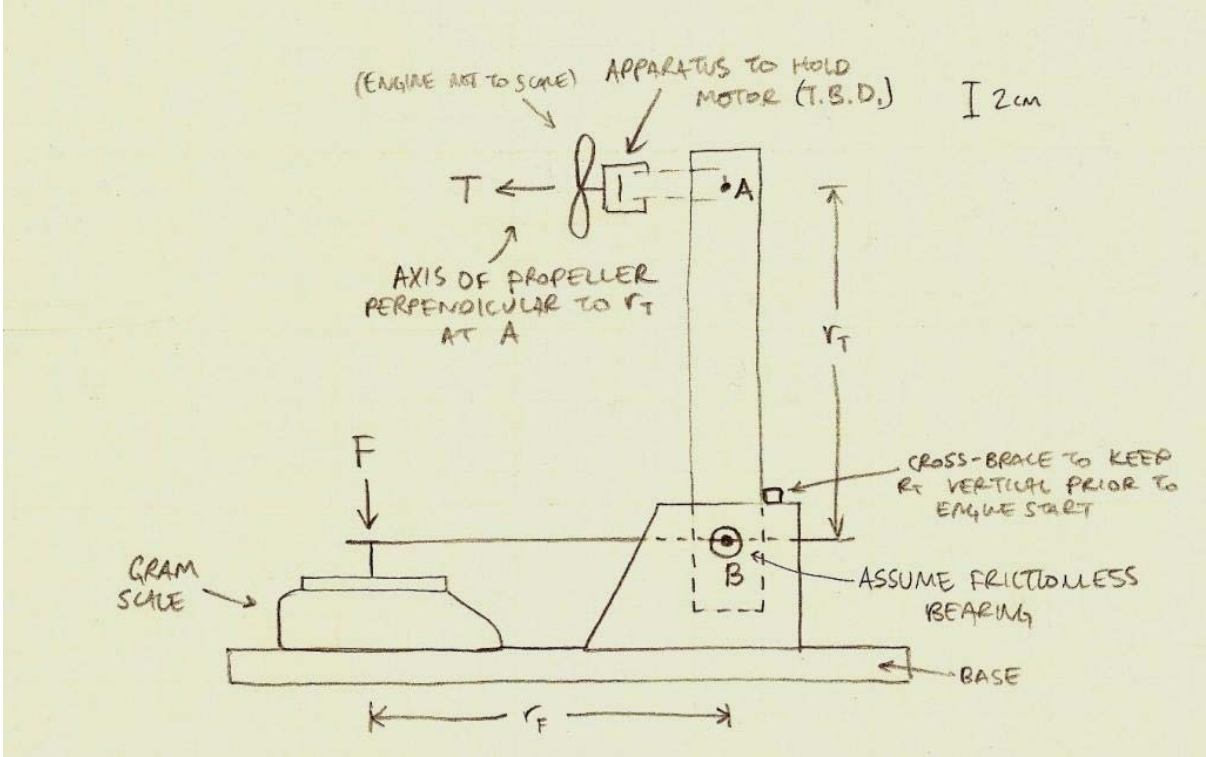

Figure 25 : Thrust test stand concept sketch

Several online forums were visited to explore popular concepts in the community of remote controlled aircraft. All of the concepts utilized simple moment arms and scales to accomplish the testing, but one particular configuration was clearly preferred. This setup was chosen for the IARC thrust stand.

The specific design of the stand (shown in Figure 25) uses the popular "L" shaped structure mounted on a pivot point. On the upright part of the structure, a motor was mounted perpendicular to the fixture, creating a moment arm. The horizontal part of the structure became a second moment arm, into which was drilled a screw. As the structure pivoted about the fulcrum, the screw pressed down on a gram scale. The distances from the pivot point to the screw (r_F in figure) and to the shaft of the motor (r_T in figure) were equal; therefore the amount of thrust generated by the spinning propeller translated exactly to the equivalent amount of mass that can be lifted.

The stand was constructed of ¼" Poplar wood so that it would be sufficiently rigid for the thrust testing. The pivot point was created from a lightweight metal tube around a metal rod. The dimensions of the tubing were just large enough so that the fixture easily rotated on the rod

without any lateral motion. The scale used was an American Weight AMW-2000 Digital Bench scale with an uncertainty of 0.05g.

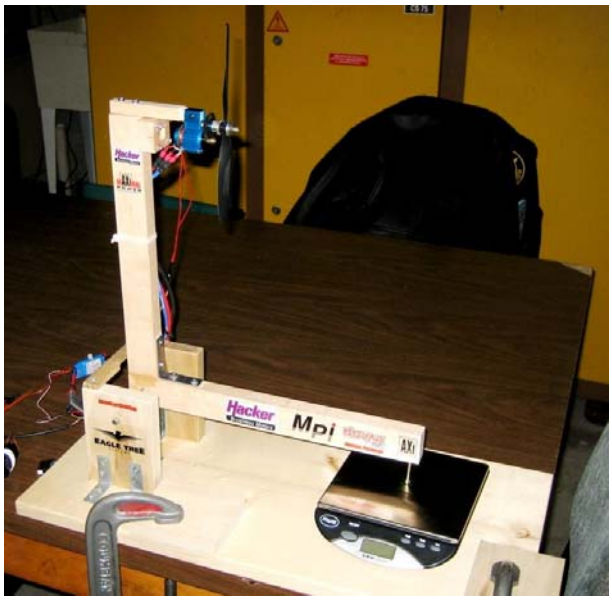

Figure 26 : The completed thrust stand

The thrust test stand was constructed at the Unmanned Systems Lab on Plantation Road, before being moved to the Virginia Tech Airport. The completed stand is shown in Figure 26.

Tests were performed to prove the concept of the stand by rotating the entire apparatus 90 degrees, hanging known objects on the thrust moment arm, and checking the mass displayed by the scale. The results of the calibration tests are shown in Table 8. The results of the tests proved that the actual mass of the object (equivalent to thrust during testing) was 1.06 times that measured by the scale. Because combinations of motors and propellers need to generate a range of thrusts instead of a specific value, it was decided that the calibration could be assumed to be 1.

Table 8 : Data used in calibration of thrust test stand

NEW PIVOT POINT METHOD - Pivot Sleeve						
Object	Measured (g)	Actual (g)	Difference (g)	% Difference	Corrected Measured (g)	Corrected % Difference
1	126.6	135.6	9	6.6	134.20	-1.0
2	263.1	281	17.9	6.4	278.89	-0.8
3	335.2	350	14.8	4.2	355.31	1.5
4	375.6	399.2	23.6	5.9	398.14	-0.3
5	447	475.3	28.3	6.0	473.82	-0.3
6	577.9	610.7	32.8	5.4	612.57	0.3
7	857.6	895.8	38.2	4.3	909.06	1.5

5.7.2 Eagle Tree Systems Data Logger

In order to record various parameters during motor testing, the Eagle Tree Systems eLogger V3 was used. This data logger monitored the battery voltage, the current draw of the

motor, the RPM of the motor, the amount of current used in mAh, as well as two temperatures. Data was recorded on a laptop through the use of a USB cable. Figure 27 shows a screen shot of actual testing conditions. The data logger was placed between the battery and the ESC to measure these values. The eLogger V3 was capable of handling up to 70 volts and/or 100 amps [12]. The component setup is outlined in Figure 28.

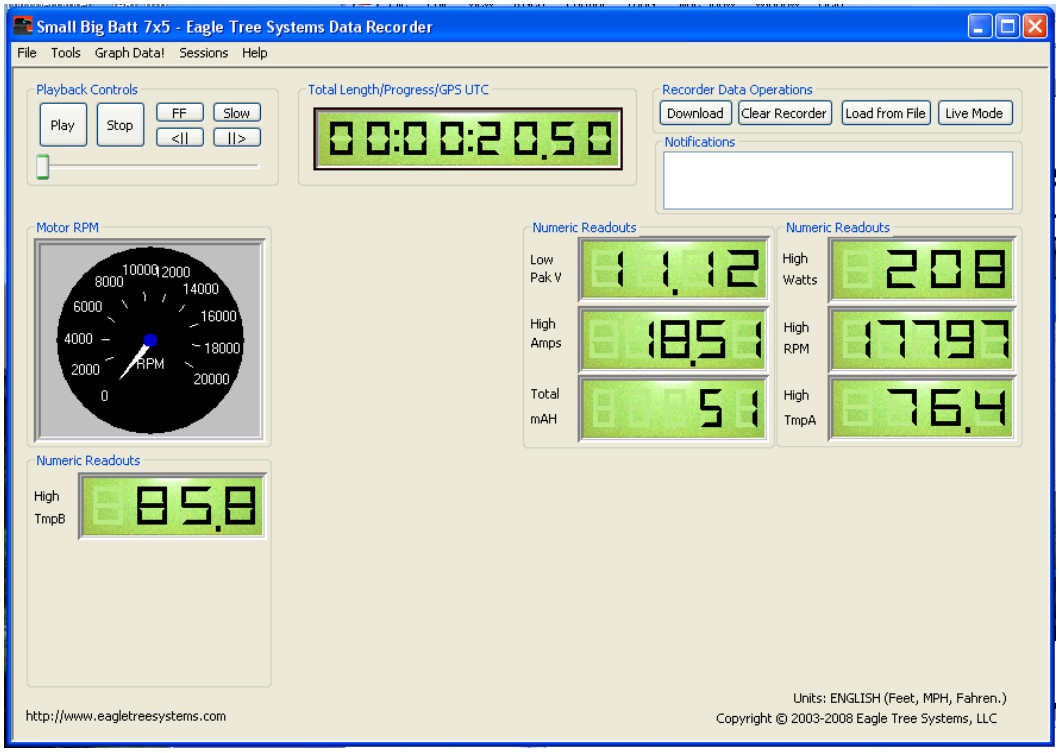

Figure 27 : Screenshot of Eagle Tree Systems eLogger V3 during testing

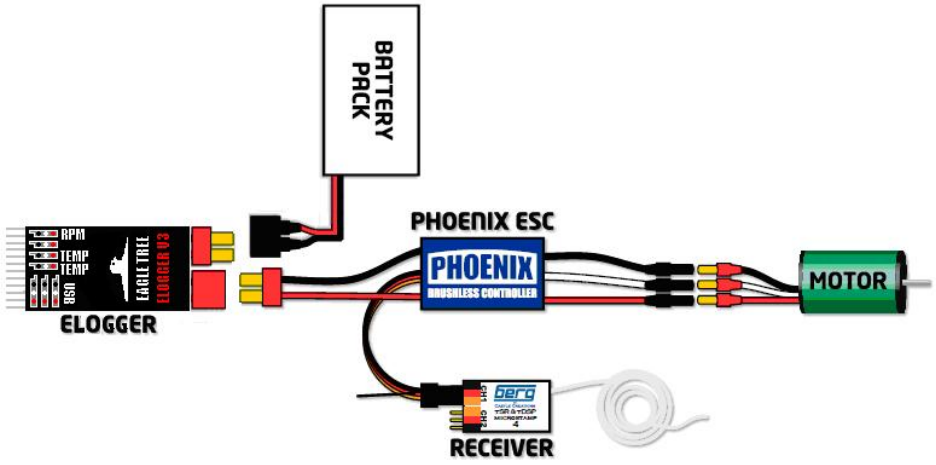

Figure 28 : Component setup used in testing (Picture adapted from Castle Creations, Inc.)

5.7.3 Test/Safety Procedures

Prior to the start of motor testing, a specific test procedure was established to ensure efficiency and safety during the testing process.

The first step of the procedure was to check that the switch on the Electronic Speed Controller (ESC) was set to the "Off" position. The throttle on the controller was likewise checked to ensure that the throttle was set to zero. The propeller was checked to make sure that it was securely attached to the motor and would not come off even at high RPM. The wiring between all of the various components were checked to ensure that all connections were secure and that all wires and sensors were clear of the propeller's range of rotational motion.

Safety glasses and long-sleeved shirts or jackets were worn during all testing to prevent injury in the event that a propeller came loose. A sheet of foam was also placed between the thrust test stand and the individuals running the test as an extra level of protection.

With the safety equipment in place, the data logger was connected via USB cable to the laptop used to record the test results. The scale was turned on and the "Tare" button pressed to eliminate the forces and moments naturally generated by the configuration of the test stand. The controller was turned on, so that it could begin transmitting to the receiver. The switch on the ESC was flipped to provide power to the ESC and send signals from the receiver to the motor. To acknowledge that the connection was completed, the ESC would emit a series of beeps.

Once the audio confirmation had been given, the throttle on the controller was increased to an initial low speed. This first increment of speed was used to check the rotation direction of the propeller. If the propeller was spinning in the correct direction, the downwash from the propeller could be felt behind the motor. If the propeller was spinning in the opposite direction, the downwash could not be felt, and the test was suspended until the leads connecting the motor to the ESC were reversed.

Once it was confirmed that the propeller was spinning in the correct direction, the throttle was gradually increased to its maximum value. Data concerning the motor RPM, battery pack voltage, current draw, and thrust generated were retrieved from the data logger and scale and recorded by hand into Microsoft Excel. Once the data was recorded, the throttle was once again returned to zero and the process was restarted for the next combination of motor and propeller.

5.7.4 Test Results

The main goal of the thrust tests was to find a combination of motor and propeller which satisfied the maximum thrust requirement of 570g with the lowest amp draw possible. The

Hacker A10-9L (the smallest Hacker motor) was tested first. The preliminary tests were performed using the Thunderpower 7.4V 2100 mAh LiPo battery at full throttle. The results are summarized in Table 9.

Table 9 : Test results for A10-9L motor using 7.4V battery

Motor weight with wires and prop adapters (g): 24.9
Battery Weight (g): 100.3

Prop Size	Pack Volts (V)	Amp Draw (A)	RPMs	Thrust (g)	Watts	Weight (g)
APC 6x4 TE	8.02	6.7	11200	220	52	4.6
APC 7x5 TE	7.9	10.6	9300	335	81	8.1
GWS 6x3	8.07	4.9	12100	208	40	2.1
APC 5.5x4.5 TE	8.03	5.7	11600	180	45	4.2
APC 5x5 TE	8	5.5	11700	121	44	3.5
APC 4.75x4.75 TE	8.03	4.7	12100	112	38	3.3
APC 4.5x4.1 TE	8.03	3.8	12500	98	31	3.6
Master 6x4 Tri	7.9	7.7	10600	209	59	6.7
Master 7x4 Tri	7.8	10	9300	278	75	10.8

This particular motor only weighed 24.9g which easily satisfied the weight requirement. The best performance combination is highlighted in yellow in Table 9. This combination of the APC 7x5 Thin Electric and Hacker A10-9L motor provided 335g of thrust which is well below the required maximum thrust while drawing 10.6A; therefore, this motor drew too much current and failed to provide the required thrust. The motor was decidedly insufficient to satisfy the propulsion requirements. Another drawback to this motor was that the propeller had to be secured to the motor using an O-ring due to the small outer shell size. With four propellers spinning at over 10,000 RPM, the probability that the propeller would eventually fly off became a real possibility. For both safety and performance reasons, this motor was not chosen for any further use.

The Hacker A20-34S was the next motor tested using the 7.4V battery at full throttle. Results are summarized in Table 10.

Table 10 : Test results for A20-34S motor using 7.4V battery

Motor weight with wires and prop adapters (g): 43.3
Battery Weight (g): 100.3

Prop Size	Pack Volts (V)	Amp Draw (A)	RPMs	Thrust (g)	Watts	Weight (g)
APC 6x4 TE	7.92	5.2	12600	221	41	4.6
APC 7x5 TE	7.8	9.4	10700	362	73	8.1
APC 8x4 TE	7.7	11	9800	433	85	12.3
APC 8x4 TE (Test 2)	7.84	11.12	10100	426	87	12.3
APC 8x4 REG	7.9	10.5	10400	428	83	16.6
APC 8x6 TE	7.6	12.8	8600	428	97	12.7
APC 8x8 TE	7.47	14.8	7400	337	111	12.5
GWS 6x3	7.84	3.9	13100	191	31	2.1
APC 5.5x4.5 TE	7.8	4.7	12700	165	37	4.2
APC 5x5 TE	7.8	4.4	12800	105	34	3.5
APC 4.75x4.75 TE	7.77	3.72	13100	108	29	3.3
APC 4.5x4.1 TE	7.8	3	13500	92.6	23	3.6
Master 6x4 Tri	7.67	6.1	11900	195.7	47	6.7
Master 7x4 Tri	7.5	8.8	10500	272.3	64	10.8
Master 8x4 Tri	7.34	12.8	8300	375	92	14.5

The combination of the APC 8x4 Thin Electric propeller and the Hacker A20-34S motor performed the best with a maximum thrust of 433g. Unfortunately this thrust still falls short of the motor requirement while drawing too much current (11A). With this motor, the propeller could be securely fastened using a propeller adapter. Due to the low thrust and high amp draw this motor did not meet the requirements and was not chosen.

While the results of the APC 8x4 Thin Electric propeller and A20-34S motor combination did not quite satisfy the propulsion requirements, an endurance test was performed to determine if the current capacity of the battery was sufficient. To perform this test, using the gram scale, the thrust of the motor was held constant at 375g. The test concluded that with the APC 8x4 Thin Electric propeller and the Hacker A20-34S motor, the endurance for one motor operating on the 7.4V battery was 12.5 minutes. This endurance was found to be sufficient; however this meant that a total of four batteries were necessary, one for each motor.

The Feigao inrunner motor was also tested using a direct drive system. It was found that while this motor spun at a very high rate (5800 kV), it did not have enough torque to spin a propeller of sufficient size. This motor also tended to overheat very quickly due to large loads induced by the propeller; therefore, this motor was quickly determined to be inadequate for this application.

Initially it was thought that emphasis in motor selection should be placed on higher kV values for motors. It was believed that more thrust would be generated since the motor would be able to spin faster. However, a higher kV value for a particular motor usually resulted in less

torque and increased amp draw (subsequently decreasing endurance). To get the amp draw down to an acceptable level, that meant that the motor had to spin a smaller diameter propeller. Since the propeller diameter is a major component in the thrust equation (4), decreasing the diameter decreases the thrust. Therefore, a tradeoff between a high kV value and the propeller diameter had to be made.

Instead of choosing new motors with higher kV values, it was determined that a battery with higher voltage would have the same effect by raising the RPM of the motor since the kV rating is based on RPM/battery voltage. Using Equation 5, the endurance was approximated.

$$Runtime\ (in\ mins) = \frac{Battery\ Capacity(in\ Amps)}{Motor\ Amp\ Draw\ (in\ Amps)} * 60\ mins. \qquad (5)$$

Equation used for endurance calculations

The Thunderpower 11.1V 2600 mAh battery was chosen during the second iteration of batteries due to its large energy density compared to other available LiPo batteries currently on the market. The battery was chosen with a larger capacity since the capacity of the 7.4V, 2100 mAh battery did not provide a long enough endurance time. At this point a viable motor solution was yet to be found, so the endurance could not have been accurately predicted.

The next logical step was to retest the Hacker A10-9L and Hacker A20-34S motors with the 11.1V battery. The results of testing the A10-9L motor are shown Table 11:

Table 11 : Test results for A10-9L motor using 11.1V battery

Motor weight with wires and prop adapters (g):	24.9
Prolite 2 2600 mAh Battery Weight (g):	185.8

Prop Size	Pack Volts (V)	Amp Draw (A)	RPMs	Thrust (g)	Watts	Weight (g)
APC 6x4 TE	11.4	11.7	14000	375	140	4.6
APC 7x5 TE	11.22	17	11300	530	176	8.1

Since it was previously found that the APC 7x5 Thin Electric propellers had performed the best with the A10-9L motor, this propeller was tested first. This combination provided over 500g of thrust but still did not satisfy the thrust requirement. The motor also drew 17A during testing which far exceeds the requirements. Next a smaller propeller was tested and found to be unsatisfactory. The small motor was finally crossed off the list of possibly motor solutions.

The Hacker A20-34S was tested as well with the 11.1V battery at full throttle. The results are summarized Table 12.

Table 12 : Test results for A20-34S motor using 11.1V battery

Motor weight with wires and prop adapters (g): 43.3
Prolite 2 2600 mAh Battery Weight (g): 185.8

Prop Size	Pack Volts (V)	Amp Draw (A)	RPMs	Thrust (g)	Watts	Weight (g)
APC 6x4 TE	11.7	10.6	17100	395	225	4.6
APC 7x5 TE	11.4	12.6	13700	570	171	8.1
APC 8x4 TE	11.39	18.4	12700	670	209.576	12.3
APC 8x6 TE	11.09	20.4	10200	630	216	12.7
Master 6x4 Tri	11.7	11	16600	405	127	6.7
Master 7x4 Tri	12.2	14.7	14200	570	162	10.8
Master 8x4 Tri	11.2	20.2	10200	660	215	14.5

It was found that the APC 7x5 Thin Electric, APC 8x4 Thin Electric, APC 8x6 Thin Electric, Master 7x4 Tri-blade, and Master 8x4 Tri-blade propellers all satisfied the given maximum thrust requirement of 570g. The best solution in this case turned out to be the APC 7x5 Thin Electric propeller since the amp draw with this propeller was the lowest at 12.6A; however this is still above the propulsion requirement of less than 10A at maximum thrust. The next step in the testing was to perform hover endurance testing. Using the APC 7x5 Thin Electric propeller, the thrust was set to a constant 375g and the endurance was measured. This particular motor and propeller combination ran for 13 minutes. While this is sufficient, it would again require one battery for each motor. Hover endurance test results are shown in Table 13.

The largest Hacker motor, the A20-30M, was tested next. While this motor pushes the upper limit of the weight requirements, it was determined that this would be acceptable if the performance advantages outweighed the weight disadvantages. This motor was tested with a variety of propellers using the 11.1V battery at full throttle. Test results are summarized in Table 14.

Table 13 : Hover endurance tests with 7x5 TE propeller

Hover Endurance - APC 7x5 TE (11200 RPMs)		
Thrust (g)	Pack V (V)	Time (min)
380	11.7	:30
419	11.47	1:20
407	11.39	2:00
401	11.27	3:00
393	11.17	4:00
391	11.09	5:00
386	11	6:00
380	10.9	7:00
379	10.86	8:00
372	10.79	9:00
370	10.74	10:00
408	10.63	11:00
404	10.48	12:00
383	10.2	13:00

Table 14 : Test results for A20-30M motor using 11.1V battery

Large Motor (11.1V) - All values at 100% throttle

Motor weight with wires and prop adapters (g): 52.8
Prolite 2 2600 mAh Battery Weight (g): 185.8

Prop Size	Pack Volts (V)	Amp Draw (A)	RPMs	Thrust (g)	Watts	Weight (g)
Master 8x6 Tri	11.9	12.5	10300	650+	149	14.5
Master 7x4 Tri	12.1	7.6	12100	370	92	11
APC 7x5 TE	12.05	7.7	12000	430	93	8.1
APC 8x4 TE	11.9	9.4	11300	540	112	12.6
APC 11x8 TE	11.4	22.3	7200	880	254	21.2
APC 9x4 REG	11.7	11.2	10600	690	131	22.6
APC 8x6 TE	11.7	12.7	10300	555	149	12.5
APC 8x8 TE	11.7	14.8	9500	475	173	12.5
APC 8x3.8 SF	11.47	9	10800	575	103	7.4
APC 8x3.8 SF (Test 2)	11.9	9.32	11000	562	111	7.5
APC 8x3.8 SF P	11.9	9.6	10900	585	114	7.1
Great Planes 8x6 SF	11.11	12.4	8900	600	138	6.3
APC 9x6 TE	11.11	12.6	9300	680	140	17.8
APC 8x4 SRT	11.36	8.1	11000	494	92	16.7
Great Planes 8x4	11.34	6.9	11500	454	78	5.3
Master 8x4	11.29	9.5	10600	449	107	10.2
APC 7.8x6 CF	11.16	9.9	10300	530	110	14.1
Dragonfly 8x4.5	11.9	12.5	10000	645	149	5.6
Dragonfly 8x4.5P	11.9	12.3	10100	620	146	5.5
Walkera 7.5 Rotor	11.72	7.8	11400	370	91	4.3
XUFO-1 Rotor	12	6.5	11000	260	78	5.6

As can be seen from the table, there were many propellers that satisfied the maximum thrust requirement using this motor. The best performing propeller was found to be the APC 8x3.8 Slow Flyer propeller which provided 575g at maximum thrust and only drew 9A. A hover endurance test was performed with this combination, during which it was found that this combination of motor and propeller provided a runtime of over 26 minutes (see Table 15 and Figure 29). This meant that two motors could be run off of one battery thereby drastically reducing the overall vehicle weight. A viable motor and propeller combination was finally found that satisfied the maximum thrust requirement of 570g, an endurance of more than 10 minutes, and an amp draw of less than 10A. It was also observed that there was a difference between the tractor and pusher version of the APC 8x3.8 Slow Flyer propellers. The pusher version of the propeller weighed slightly less, and at the same amp draw, the pusher propeller produced less thrust than the tractor version of the propeller. This was important to note and will have to be accounted for in the controls algorithms.

Table 15 : Hover endurance results for A20-30M motor using APC 8x3.8 Slow Flyer propeller

Hover Endurance - APC 8x3.8 SF(~9000 RPMs)			
Thrust Measured (g)	Thrust Corrected (g)	Pack V (V)	Time (min)
385	408	12.12	:30
375	398	12	1:00
373	395	11.9	2:00
366	388	11.8	3:00
356	377	11.69	4:00
356	377	11.59	5:00
350	371	11.52	6:00
400	424	11.39	7:00
397	421	11.31	8:00
392	416	11.26	9:00
390	413	11.19	10:00
391	414	11.14	11:00
388	411	11.09	12:00
377	400	11.06	13:00
384	407	11.01	14:00
380	403	10.98	15:00
381	404	10.96	16:00
378	401	10.93	17:00
379	402	10.91	18:00
377	400	10.88	19:00
377	400	10.86	20:00
375	398	10.83	21:00
371	393	10.78	22:00
367	389	10.71	23:00
367	389	10.58	24:00
352	373	10.33	25:00
353	374	9.6	26:00

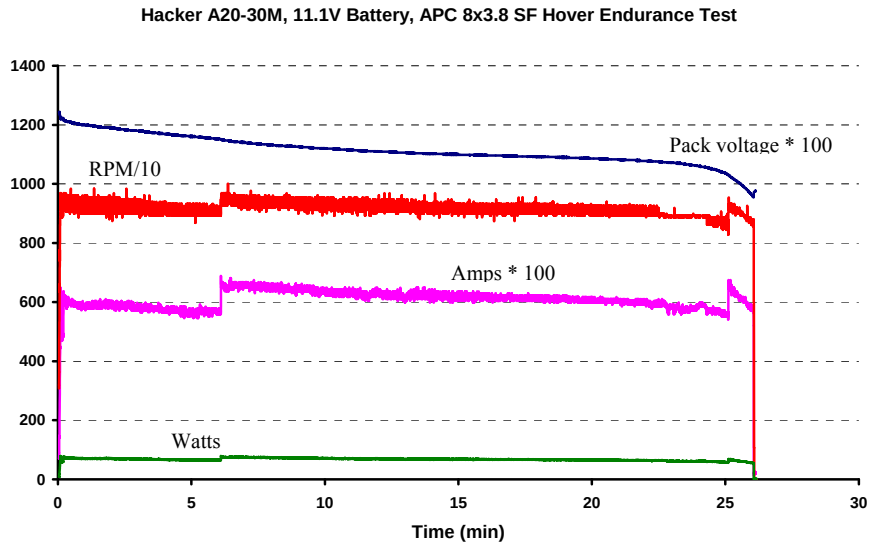

Figure 29 : Hover endurance test results for A20-30M motor using 11.1V battery and APC 8x3.8SF propeller

Table 16 : Test results for HiMax 2015-3666 motor using 11.1V battery under different gearing scenarios

Motor weight with wires and prop adapters (g): 66.7
Prolite 2 2600 mAh Battery Weight (g): 185.8

4.4:1 Gear Ratio						
Prop Size	**Pack Volts (V)**	**Amp Draw (A)**	**RPMs**	**Thrust (g)**	**Watts**	**Weight (g)**
Master 8x6 Tri	11.82	7.9	7600	445	93	14.5
APC 8x4 TE	11.98	5.85	8300	395	70	12.6
APC 11x8 TE	11.32	13.6	5500	650	154	21.2
APC 9x4 REG	11.77	7.5	7800	500	88	22.6
APC 8x6 TE	11.8	8.16	7600	430	96	12.5
APC 8x3.8 SF	12.05	6.49	8250	442	78	7.4
Great Planes 8x6 SF	11.77	9.5	7100	500	112	6.3
APC 9x6 TE	11.64	9	7100	550	105	17.8
APC 7.8x6 CF	11.9	7.2	7900	425	86	14.1

6.6:1 Gear Ratio						
Prop Size	**Pack Volts (V)**	**Amp Draw (A)**	**RPMs**	**Thrust (g)**	**Watts**	**Weight (g)**
Master 8x6 Tri	11.87	3.79	6000	244	45	14.5
APC 8x4 TE	11.93	2.5	6200	220	30	12.6
APC 11x8 TE	11.55	8.1	5000	520	94	21.2
APC 9x4 REG	11.8	3.4	6000	287	40	22.6
APC 8x6 TE	11.8	3.7	6000	242	44	12.5
APC 8x3.8 SF	11.85	2.44	6100	214	29	7.4
Great Planes 8x6 SF	11.72	4.43	5800	329	52	6.3
APC 9x6 TE	11.72	4.3	5800	360	50	17.8
APC 7.8x6 CF	11.77	3.4	6000	215	40	14.1

Additional research was performed and it was found that multiple quadrotor designs employed the use of a geared propulsion system. It was originally thought that the gearing would reduce the load on the motor which in turn would decrease the amp draw of the motor and increase flight endurance. The HiMax 2015-3666 geared system was chosen and tested. This motor was also slightly overweight, but if the advantages outweighed the disadvantages, it would be a possible motor solution. The results of the thrust tests are shown in Table 16.

The geared system initially came with a 6.6:1 gear ratio and this was tested first. It was found that the APC 9x6 Thin Electric propeller yielded the most thrust; however it was still well below the thrust requirement. It was concluded that the propeller was not spinning fast enough to generate the required thrust because of the high gear ratio. The gears were changed so that the gear ratio was 4.4:1. The test was repeated and the APC 9x6 Thin Electric provided almost 570g of thrust while drawing only 9A. This motor and propeller therefore performed up to the same standard as the Hacker A20-30M and APC 8x3.8 Slow Flyer propeller. The drawbacks to the geared system led it to not be chosen with these being the added weight of the geared system, the larger propeller diameter, and the added complexity.

It was concluded that the Hacker A20-30M motor along with the APC 8x3.8 Slow Flyer propeller provided the best combination of thrust, amp draw, and weight and was chosen to be installed on the first prototype. Additionally, the Thunderpower 11.1V 2600 mAh batteries (2) were selected to be used in the first prototype along with the Castle Creations Phoenix-25 ESC.

5.7.5 Motor and Electronic Speed Controller Failures

During testing, failures of the ESC and the Hacker A20-30M motor occurred. At one point during testing, the transmitter was turned on and the throttle was increased. Upon increasing the throttle, the motor suddenly stopped rotating and quickly overheated. The increase in temperature caused the motor to start smoking. Shortly after the motor started smoking, the Castle Creations Phoenix-10 ESC caught fire. The battery was quickly removed from the ESC and the components were allowed to cool down. After inspecting the motor, it was determined that one of the wires in the motor windings had broken and short circuited the motor. When this happened, the current running through the motor essentially became infinite. Since the speed controller was only rated to handle peak loads of 15A, with the infinite current, it subsequently overloaded and caught fire. It was concluded that the motor failed first, which in turn caused the ESC to fail.

During testing it was also noted that when the motor was running at maximum throttle, the ESC began to heat up and limit the current going to the motor. At maximum throttle the motor draws between 9 and 10A. The current limiter on the ESC began to limit current around 10A. Based on these observations, it was concluded that increased resistance to spikes in amp draw, a lower operating temperature, and a higher rated current loading were necessary. The Phoenix-25 solved all of these problems with the only drawback being an increased mass of 10g per ESC.

The addition of a fuse in between the battery and the ESC was also investigated. The theory behind this was that the fuse would blow upon a sudden spike in amp draw and protect the motor, ESC, and battery. After a consultation with a technical representative of Castle Creations, it was determined that this would not be effective. All of the Castle Creations ESCs are equipped with a current limiter which responds in microseconds to spikes in amperage. The fastest responding fuses blow in milliseconds. Therefore, the ESC would limit the current before the fuse and thus the fuse would never blow if the ESC was functioning properly. In the failure described above, the spike of infinite current happened so quickly and was so overpowering that the current limiter stood little chance in protecting the ESC. The idea of installing a fuse between the battery and the ESC was abandoned.

5.8 Interference Testing

5.8.1 Interference Testing

One concern of the multi-propeller aircraft was the possibility of aerodynamic interference between the propellers. If the propellers are spaced too close together without any form of division or shroud, there is the possibility that the aerodynamic interaction between the propellers could cause a decrease in the total performance of the aircraft. While this possibility has been briefly acknowledged in design considerations for other small quadrotor aircraft, no specific examination of the effects could be found; therefore tests needed to be conducted to determine the minimum space necessary between the motors.

The thrust stand previously described in Section 5.7 was modified for this new form of testing. The physics of the apparatus were maintained in that the motors were mounted such that the thrust created by both motors would still translate directly to the mass displayed on the scale.

A triangle frame was constructed of 3/8" basswood to support the added weight of a second motor and ensure that the relative distances would not change even at thrust loads (Figure 30). The horizontal portion of the frame allowed for the distance between the motors to be varied so that any drop in performance with decreasing distance could be evaluated. The signal from the controller was split from the receiver so that each motor received the same and equal throttle command signal. The data logger was also attached such that the total amp draw of the two motors could be measured.

The two propellers used in each run of the experiment rotated in opposite directions (one pusher, one tractor) to represent the behavior of adjacent propellers on the actual vehicle. This created an extra step in the testing procedure, to make sure that the leads on both motors were connected such that both motors produced positive thrust. After checking the direction of rotation of both motors, the throttle was steadily increased on the controller until the two motors produced a set amount of thrust. The battery pack voltage and current draw were then recorded as a method of performance comparison.

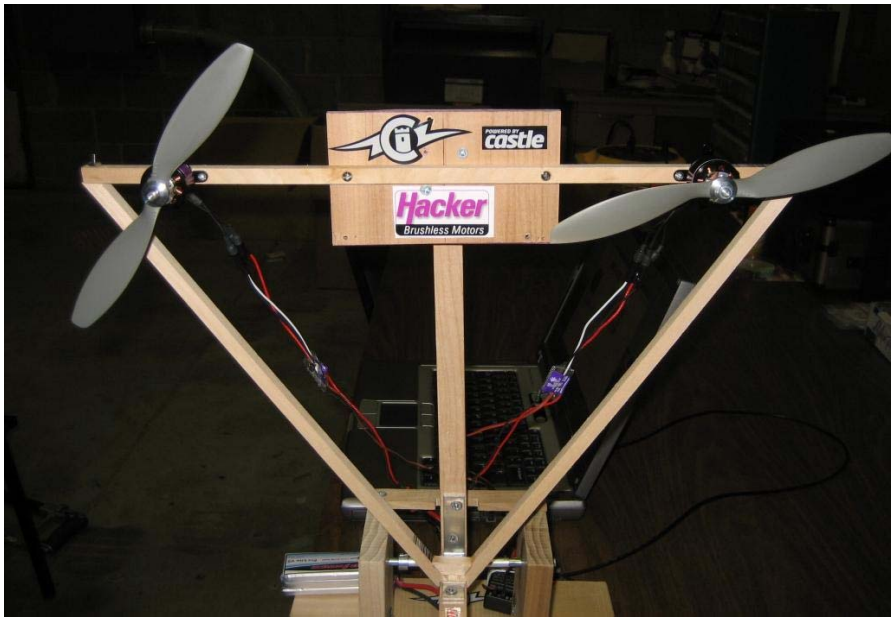

Figure 30 - Thrust stand modification for propeller interference testing

5.8.2 Results

The first run of the interference tests were conducted with the motors spaced 12.5 inches apart (measured as the distance between the two shafts of the motors). The throttle was increased until the two motors produced a combined thrust equal to 788g. The pack voltage at this thrust level was 11.8V, while the amp draw was 11.9A. Manually feeling the downwash of the two propellers, a clear "break" existed between the two downstream flows, from which it was concluded that the two propellers could not be interfering with one another at this distance.

The two motors were then spaced so that only 1 inch was left between the propeller blades (9 inches between the shafts of the two motors). This distance was chosen as this was the closest possible distance between the centerlines of the two motors without the propeller tips touching. The throttle was again increased until the motors produced a combined thrust equal to 800g. The pack voltage at this thrust was 11.36V with a current draw of 16.4A.

The difference in the two tests showed that a drop in performance occurred with shorter distance between the motors. At the same thrust generation, the two motors drew much more current when only 1" of distance separated the propellers. This proved that some form of interference occurred, and that further testing might be necessary to determine an optimal distance between motors.

Upon further inspection of the interference stand, it was decided that the stand itself may have caused some structural interference and lowered the combined performance of the two

motors. Part of the mount constructed when attaching the new frame to the old stand involved a 5.5" wide section of Maple board (Figure 30). When the motors were spaced at 12.5 inches this board was not directly underneath the propeller downwash. Upon moving the motors to a spacing of 9 inches, this board may have easily interfered with the aerodynamics of the two motors and caused the drop in performance since it was directly in the propeller downwash. This possibility was deemed not critical to the construction of the first prototype, but noted as a concern that required further investigation.

Another product of the interference testing was the realization that the downwash from the propellers might be used to cool the ESCs during vehicle operation. Temperature sensors were fixed to the ESCs during operation, and it was observed that the temperature of the speed controllers decreased from the room temperature value when the propellers were rotating.

5.9 First Prototype

5.9.1 Proto1 Construction

The following hardware selections were made for the first prototype:

- Four Hacker A20-30M Brushless Outrunner motors
- Four Castle Creations Phoenix-25 Electronic Speed Controllers
- Two Thunderpower 11.1V 2600 mAh Lithium Polymer batteries
- Four APC 8x3.8 Slow Flyer propellers (two pusher, two tractor)

Since the flight controls for the vehicle were not established at the time of the construction of the first prototype, the vehicle was controlled using the same controller/receiver combination used in the thrust testing. The throttle signal from the receiver was split four ways leading to each of the four ESCs so that each motor would receive an identical throttle command. The four ESCs were then mounted such that the downwash from the propellers would cool them during vehicle operation.

Each of the two Lithium Polymer batteries supplied battery power to two adjacent motors, spinning in opposite directions. The ESCs used did not have switches to easily allow them to be turned off when the controller was not transmitting signals; therefore the leads from the motors were arranged on the prototype such that they could easily be connected and disconnected.

5.9.2 Hover Testing

Figure 31 - First prototype tethered down for safety purposes

The initial test of the first prototype was conducted to prove that the hardware selected could lift the maximum allowed competition mass of 1.5 kg. As mentioned in Section 5.1, attitude controls had not yet been implemented at the time of the construction and first flight; instead, the same throttle signal was sent to each of the four motors. Due to the nature of the ESCs and motors, it was expected that this would cause uneven thrust performance across the four propellers and therefore uneven lift and unstable movement in pitch, roll, and yaw.

To prevent damage to the craft during operation while still proving the lift capability of the prototype, the craft was tethered to a sheet of 0.5 inch thick Plywood. Holes were drilled in the plywood, and lengths of string were tied from the holes to bolts on each side of the vehicle (Figure 31). The lengths of string were determined such that the vehicle could only lift 0.5 inch off of the Plywood surface and that only slight yawing was allowed.

Once it was determined that the vehicle was secured, a procedure similar to that used in the thrust testing was followed. All electrical connections, propeller and motor mounts, and

tethers were checked, and safety equipment was placed appropriately. The controller was turned on, followed by the connection of the battery leads, completing the circuit and sending power to the ESCs. The throttle was slowly increased to a low speed so that propeller rotation direction could be checked. Upon confirmation that the propellers were spinning in the correct direction, the throttle was gradually increased again until the vehicle began to move.

As expected, the movement of the prototype was erratic and uncontrolled. The vehicle pulled at the tethers holding it down to the table, yawing and rolling under the different forces caused by the four motors. The throttle was held steady for approximately 15 seconds before being reduced again to zero and the test was ended to prevent damage to the vehicle.

Because of the behavior of the craft and the tension observed in the tethers, the hover test was determined a success. Without flight controls, a sustained hover was never observed; however, the movement that was observed was enough to prove that the propulsion system in its most crude form provided ample thrust to move the vehicle.

5.9.3 Ground Effect Testing

A question regarding the effect of the propeller downwash on the stability of the vehicle was raised during testing. To investigate the effects of the downwash, the thrust fixture was used. A large sheet of plywood was used to simulate the ground. The plywood was held vertically behind the thrust fixture in a parallel plane to the propeller. It was first placed six inches away from the propeller to determine if the thrust would increase or decrease because of the presence of the "ground." Table 17 below shows the results of this testing. As can be seen, there was a very minor deduction in thrust at ground clearances less than 1.5 feet. However, the difference of 20 or 30 grams is only a change of 4% in the overall thrust. Therefore, it was concluded that for this vehicle there is not a significant ground effect and any changes in thrust would occur at a ground clearance of 1.5 feet or less. For the duration of the mission, the vehicle will be flying at much higher altitudes and thus the effects of the proximity of the ground are insignificant.

Table 17 – Results of Ground Effect Testing

Initial Thrust (g)	740

Ground Clearance (ft)	Thrust (g)
0.5	710
1.0	715
1.5	725
2.0	735
2.5	735
3.0	720

Largest % change in thrust	4.05

The "wall effect" was also tested. This testing was very similar to the ground effect testing except that the sheet of plywood was held in a plane perpendicular to the propeller plane. The distance from the propeller tip to the plywood was also varied in the same manner as in the ground effect test. It was found that no reduction in thrust was observed for any clearance since the plywood was not directly in the propeller downwash. It was also noted that the presence of the wall did not induce any instabilities. Therefore, it was concluded that for this vehicle the both the wall and the ground do not cause any significant losses of thrust or any instabilities of the vehicle

5.10 Hover Test Stand

A test was performed immediately following the construction of Proto1 to prove that the propulsion system as developed could lift the maximum competition weight. The vehicle was tethered to a level surface for the test in light of the absence of any control system on the prototype. During the test, the vehicle struggled against the tethers and briefly lost contact with the table; therefore the test was deemed successful and the propulsion system proved competent for the competition requirements. It was speculated afterwards that some ground interference between the propellers of the quadrotor and the test surface may have contributed to the results of the test. A new test stand was subsequently constructed to allow for greater movement of the prototype in the vertical direction.

Figure 32 - The hover stand showing the two vertical rods attached to the wooden base.

The test stand shown in Figure 32 was constructed of a wood base and two vertical metal rods. Visible in Figure 33, the two rods pass through oversized holes in the base plate and the top of the payload box to allow the vehicle to move vertically on the test stand. The choice was made to use two rods to limit the movement of the vehicle to only vertical motion and prevent unwanted rotational or translational motion.

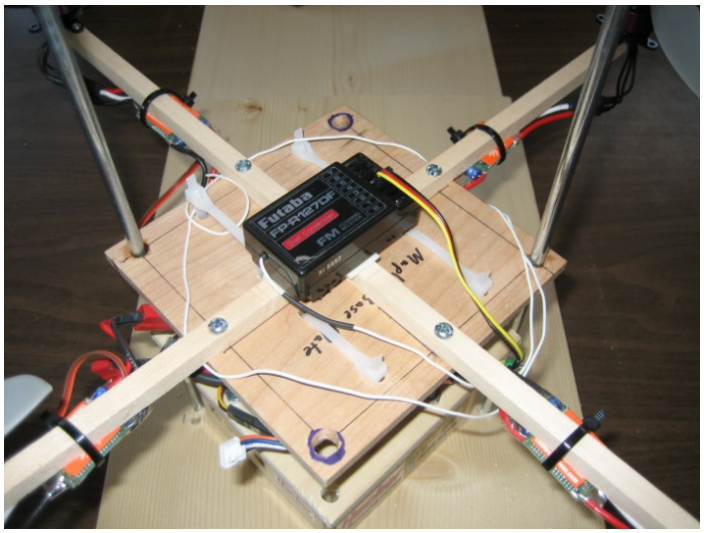

Figure 33 - Close-up of the test stand showing the two rods passing through the vehicle.

A wood block was fixed to the top of the stand to hold the rods in place and to prevent the vehicle from inadvertently leaving the test stand. Shaft collars were placed on the rods above and below the wood block to hold the block in place.

Using a remote control transmitter, the propulsion system was engaged and the throttle signal sent to the motors was increased. The vehicle left the wooden base and moved up the vertical rods with ease. The throttle was held at a steady value, and the vehicle achieved a hover state on the test stand. Small adjustments to the throttle signal provoked sharp increases and decreases in altitude, proving the competence of the propulsion system and disproving any significant ground effects.

The stand was then dismantled and transferred to the Unmanned Systems Lab to be used for the development of the altitude control system.

5.11 Pitch and Roll Test Stand

A single degree of freedom test stand was built to isolate testing of the pitch or roll control algorithms. This was accomplished by restricting the translational and rotational (about the *z axis*) motion of the vehicle. Using this test stand, only roll or pitch can be tested at one time. Before a test stand was constructed, the location of the center of gravity (CG) was located. An approximate location was given by the structures team using Autodesk Inventor. A test stand was then designed so that the pivot axis and the CG would coincide. The design called for a wood tray to be cut so that the ME payload box would rest inside a cut out square of the wood tray. This tray had metal rods fixed to it so that it could rotate freely (see Figure 34 below). The wood tray was attached to the ME payload box via threaded rods. The threaded rods allowed for the wood tray to be moved vertically with respect to the ME payload box effectively raising or lowering the pivot axis of the vehicle. Therefore, if it was found that the vehicle was top heavy, this implied that the CG was above the pivot axis. The distance between the top of the ME payload box and the wood tray was decreased thereby decreasing the distance between the pivot axis and the CG. To reduce the risks of testing, the pitch/roll test stand was constructed so that the maximum rotation of the vehicle was limited to 15 degrees. Roll testing was accomplished first and then the vehicle was rotated 90 degrees to test the pitch algorithms.

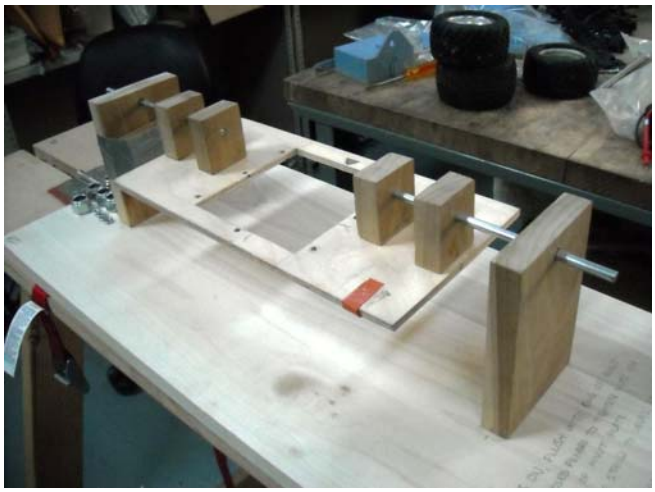

Figure 34 - Roll and pitch stand without Proto1 in place for testing.

5.12 Yaw Stand

A yaw stand was constructed to allow for the development of the yaw attitude control system. The stand consists of a wooden base, onto which was fixed a Lazy Susan Bearing. On top of the bearing was attached a square piece of wood approximately 5 inches on a side and 1/8 inch thick. This square piece of wood was covered in 1/2 inch thick strips of Velcro, arranged in a square pattern. A matching square pattern composed of the opposing sides of the Velcro strips was attached to the bottom of the payload box on Proto1. Figure 35 shows the yaw stand with its rotating element and Velcro pattern.

Proto1 could then be fixed onto the test stand via the Velcro connection so that it would not leave the test stand unless significant force was manually applied. While on the stand, the vehicle can rotate about its yaw axis, but cannot rotate or translate in any other direction.

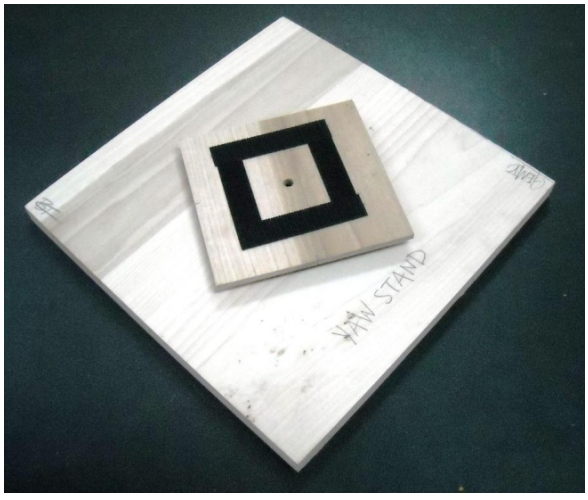

Figure 35 - Yaw stand without Proto1 in place for testing.

5.13 Future Goals

With test stands constructed for vertical motion and rotation, the continued progress of the project is now dependent on the development of the flight controls. Once those flight controls have been implemented on Proto1, the propulsion system on Proto1 will be transferred to Proto2.

The hover stand that was built might be used to more accurately test the battery endurance in simulated flights, and the results of those tests will determine whether the propulsion system in its current state is still adequate.

The propulsion team will also most likely take on the task of creating a carbon fiber payload box similar to that which was created for Proto1. The construction of such a box depends on the placement of sensors which have yet to be determined.

6.0 System Dynamics and Controls

6.1 Problem and Scope

The controls group undertook the task of controlling a quad rotor vehicle design. To complete the IARC mission successfully, the vehicle must navigate its terrain while maintaining steady, stable flight and controlled movement. The goal of the controls group was to design a robust controller prior to any vehicle flight to ensure mission success, and to accomplish this, some basics of control design must be understood.

First when designing a controller, a physical model of the system dynamics must be established. Second, control inputs are introduced into the system to provide a means for the controller to change the motion of the system; the control inputs for the quad rotor are the percent of throttle of each motor. Third, once these control inputs are introduced it is important to understand how each input will affect the motion of the system. This understanding can be attained via analysis, simulation, or testing.

Fourth, the control inputs can be changed by a certain amount attain a desired position or equilibrium motion. The controller implements these gained controls in the form of a command to the system. The plant responds to the changes in the control variables, and then a sensor detects actual motion or state of the vehicle. The error between the desired input and the actual measured input from the sensor is fed back into the controller where it adjusts the command to attain the desired input (See Figure 36). The controller should be designed such that the system of interest is dynamically stabilized over a period of time and remains stable.

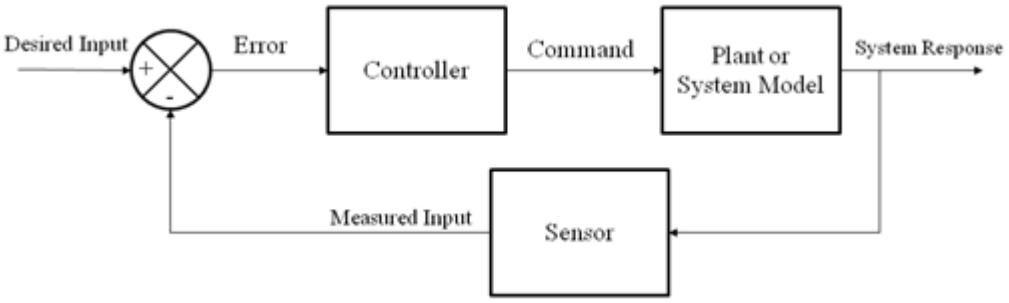

Figure 36: Basic Controls Logic Flowchart [13]

Fifth, the controller logic must be coded and developed into software. Sixth, hardware must be selected to implement the developed controller software into the actual system dynamics. Finally, the controller must be adequately tested before implementation to ensure that the control

logic is robust enough to completely characterize the system behavior and dynamically stabilize the system.

The scope of the controls team was to develop a flight controller capable of stabilizing and controlling the attitude and altitude of the quad-rotor vehicle. By controlling the attitude, the translational motion could also be controlled depending upon the desired equilibrium of the controller. The dynamic system of a quad rotor sans-controller is marginally stable at best; thus, the team worked to develop and implement a set of control loops that would successfully respond to attitude and altitude commands. To date, the controls group has developed a system model, developed controls for altitude and attitude, and is in the process of testing the robustness of these control algorithms. These works are discussed in the following sections in more detail.

6.2 Quad Rotor Dynamic System Analysis

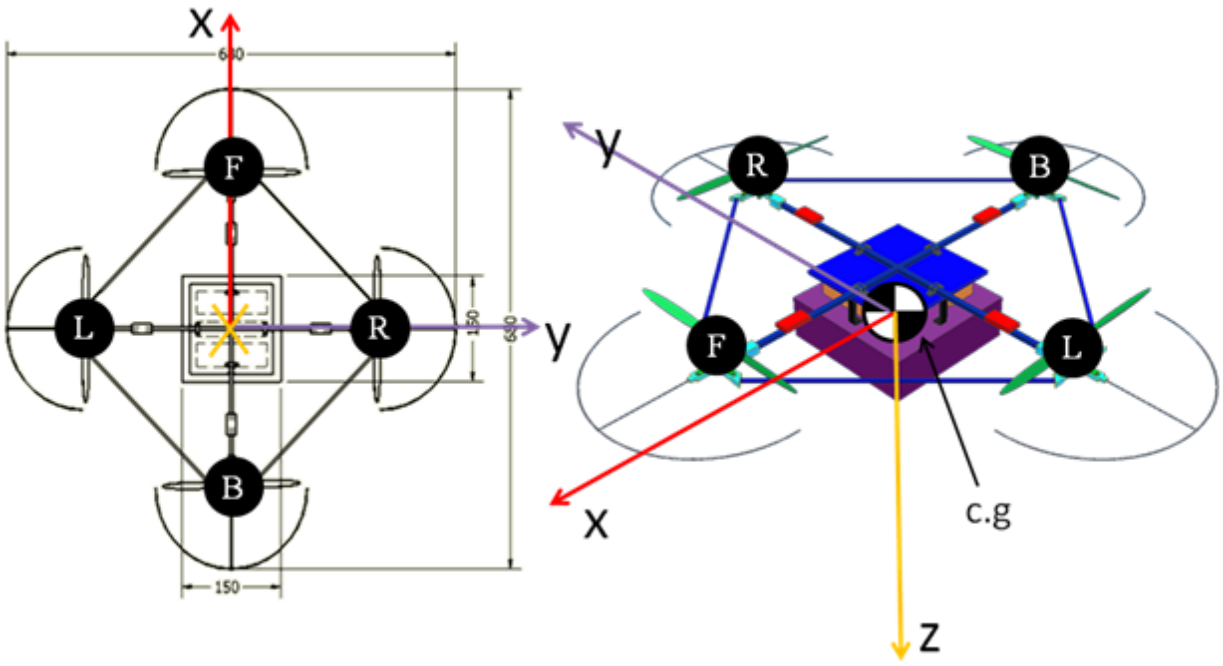

Figure 37: Quad Rotor Coordinate System and Motor Naming Convention

As in all dynamic analyses, the controls team established a coordinate system as shown in Figure 37 to help describe the motion. The x and y axes are defined by two planes of symmetry and originate from the vehicle's center of gravity (c.g.). The x-axis is pointed in the direction of positive roll and is synonymous with forward motion. Similarly the y-axis is in the direction of

positive pitch, and the z or yaw axis is formed by the cross-product of the x and y axes. This convention is analogous to the North-East-Down convention used to describe aircraft and missile dynamics. The motors are labeled F (front), R (right), B (back), and L (left) respectively in clockwise fashion.

The controls team has worked under the assumption that the quad-rotor will be operating continuously at a near hover condition. Due to the nature of the mission, the quad rotor will have to move slowly so that the blinking blue LED light can be detected; thus, small angle and small perturbation assumptions were used. With the slow motion, aerodynamic drag due to translational motion was neglected. One final assumption was that the vehicle would not move very far from the hover equilibrium, so the coupling effects of pitch and roll were neglected—products of angular rates were neglected.

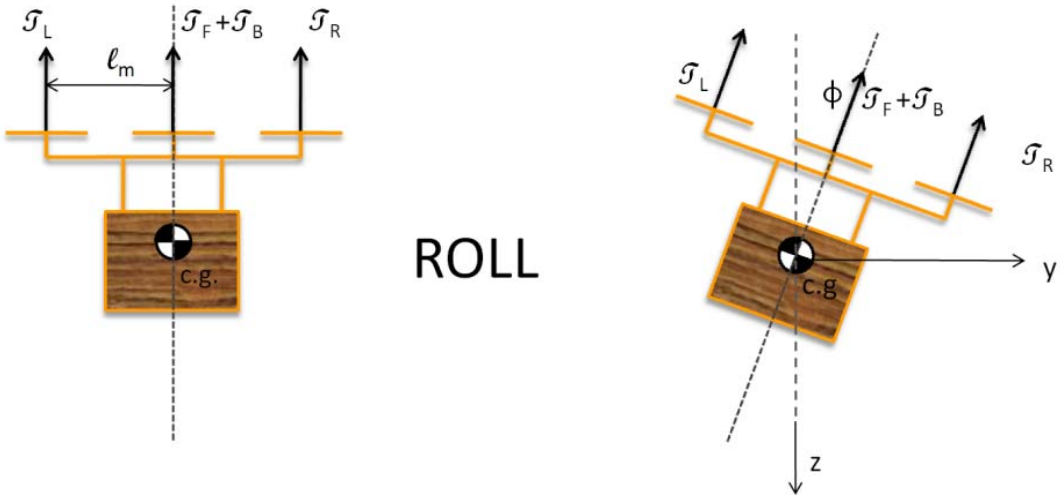

Figure 38: Roll Free Body Diagram

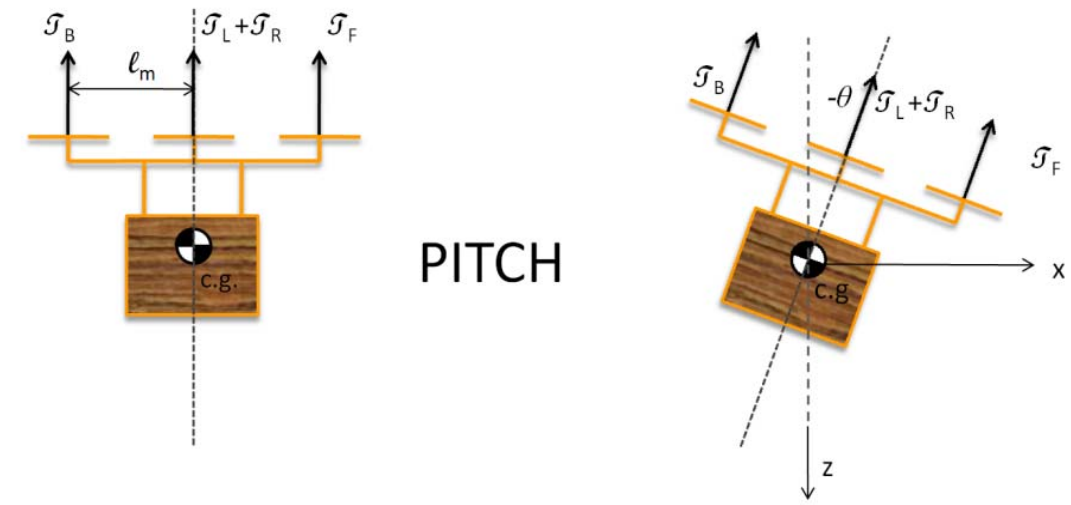

Figure 39: Pitch Free Body Diagram

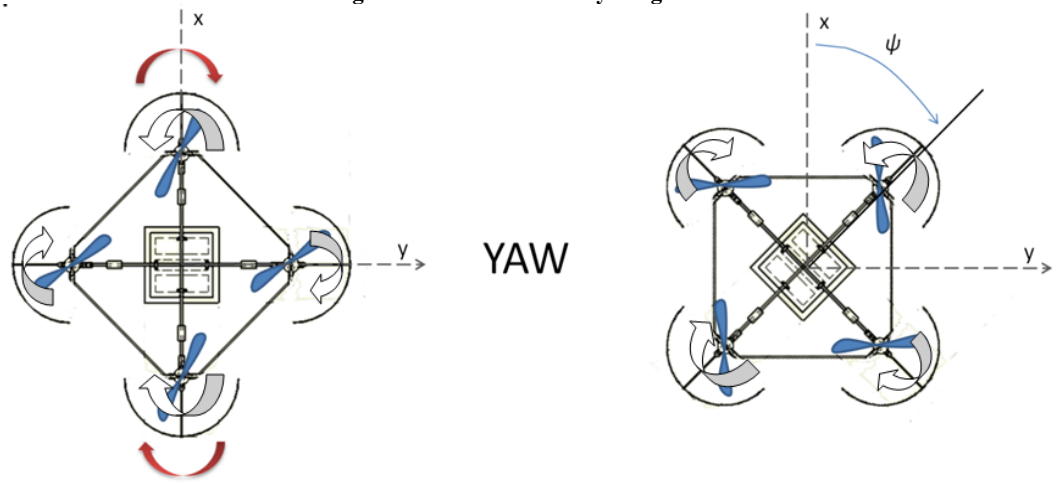

Figure 40: Yaw Diagram

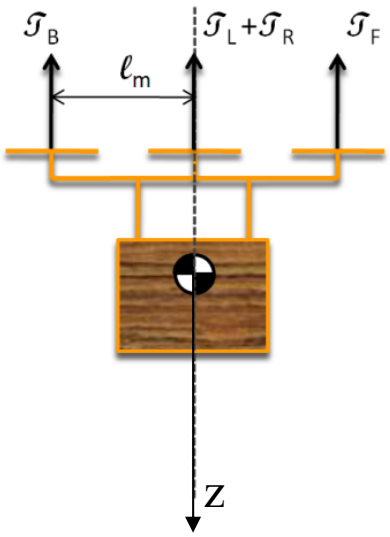

Figure 41: Altitude Free Body Diagram

Figure 38 represents a free body diagram demonstrating roll motion, where $\mathcal{T}_L, \mathcal{T}_R, \mathcal{T}_F, \mathcal{T}_B$ are thrusts due to the left, right, front, and back motors respectively. Also, l_m is the perpendicular length from each motor to the c.g. and ϕ is the roll angle. Figure 39 is the free body diagram of the pitch, where θ is the pitch angle. Figure 5 demonstrates yaw motion. The front and back propellers are rotating in the counterclockwise direction; whereas, the left and right propellers are rotating clockwise. The propeller drag operates in the opposite direction in which the respective propeller blades spin. If one were to increase the throttle to the front and back engines, the drag would eventually drive the system to rotate clockwise which is a positive yaw in the system. The rotor drag moments are proportional to the respective motor thrusts by some constant k_T. The controls group will empirically determine this constant, but for now it is estimated at 0.5. Figure 41 represents the free body diagram in the z-direction. The vehicle mass, *m*, was assumed to be 1.5 kg.

Summing the moments about the c.g. and the forces in the x, y, and z directions (Figure 38, Figure 39, and Figure 41 respectively), the following decoupled equations of motion emerge:

$$\begin{bmatrix} J_{roll} & 0 & 0 \\ 0 & J_{pitch} & 0 \\ 0 & 0 & J_{yaw} \end{bmatrix} \begin{bmatrix} \ddot{\phi} \\ \ddot{\theta} \\ \ddot{\psi} \end{bmatrix} = \begin{bmatrix} l_m & -l_m & 0 & 0 \\ 0 & 0 & l_m & -l_m \\ -k_T & -k_T & k_T & k_T \end{bmatrix} \begin{Bmatrix} T_F \\ T_B \\ T_L \\ T_R \end{Bmatrix} \tag{6}$$

Rotational Equations of Motion

$$m \begin{bmatrix} \ddot{x} \\ \ddot{y} \\ \ddot{z} \end{bmatrix} = \begin{bmatrix} -\theta & -\theta & -\theta & -\theta \\ \phi & \phi & \phi & \phi \\ -1 & -1 & -1 & -1 \end{bmatrix} \begin{Bmatrix} T_F \\ T_B \\ T_L \\ T_R \end{Bmatrix} + \begin{bmatrix} 0 \\ 0 \\ mg \end{bmatrix} \tag{7}$$

Translational Equations of Motion

Where all parameters were previously defined and small angle assumption was applied. These equations were converted to the Laplace domain (to a transfer function) via the Laplace transform, and a controller was constructed and analyzed.

6.3 Initial Control Design and Simulation

The controls team worked to design a control algorithm that would control the system attitude and altitude. The translational motion can be controlled with an attitude-altitude controller; however, a separate logic or autopilot will be designed to feed the attitude-altitude controller with desired inputs. Currently, the mechanical engineering sensors team is developing the required sensors, so it was not within the scope of the controls team this semester to develop a controller with x and y inputs explicitly; the separate navigation logic is in the controls team scope for next semester pending the sensor selection of the sensors group. The control algorithm presented below controls only attitude and altitude.

The equations of motion given above were converted to closed-loop transfer functions so that the dynamics of each state could be studied and to allow seamless controller integration into the dynamic system model (or plant). A transfer function is the ratio of the Laplace transform of the system response to the Laplace transform of the input function. The equations of motions are not readily available to convert to transfer functions. The following variables were defined in (8):

$$
\begin{aligned}
T &= T_F + T_B + T_L + T_R \\
T_{roll} &= T_L - T_R \\
T_{pitch} &= T_F - T_B \\
T_{yaw} &= T_R + T_L - T_F - T_B \\
T_z &= mg - T
\end{aligned}
\tag{8}
$$

Control Variable Equations

Where T is the total thrust, and all other variables are just dummy variables to allow for ease of computation of the transfer functions. For more information on transfer functions, consult Ogata.

With these various thrust definitions, the transfer functions were determined. Also, a PID (Proportional-Integral-Derivative) controller was implemented in each case for attitude and altitude. A PID controller was implemented because its proportional gain aspect decreases the system response time to obtain desired states, its integral gain aspect decreases steady state error, and its derivative gain aspect increases the stability of the system via damping [13].

The single-input single-output (SISO) control models for attitude and altitude were found to be:

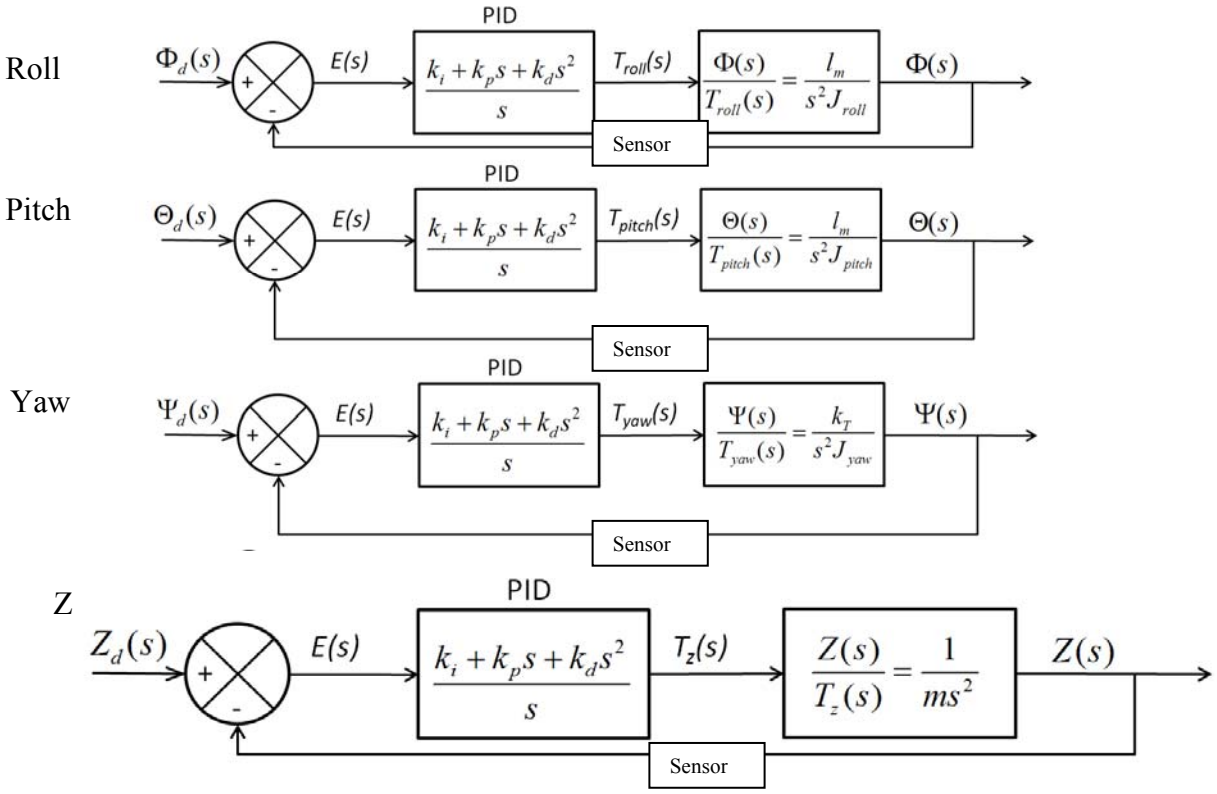

Figure 42: Attitude and Altitude Control Feedback Loops

A Simulink computer simulation of the quad-rotor vehicle dynamics was developed with the above controllers. With this simulation, the method of trial and error was used to find the appropriate gains to allow the system to achieve commanded states; this is also known as gain tuning. The above control loops were successfully able to control the roll, pitch, yaw, and altitude of the vehicle with the following gains in Table 18 below:

Table 18: Initial Control Gains

Control	K_p	K_I	K_d
Roll	100	30	10
Pitch	100	30	10
Yaw	50	0.2	10
Z	-99	-30	-100

A sample output, shown below in Figure 43, shows the predicted system response to a command to climb to an altitude of 2 m and roll right to an angle of 0.1 radians.

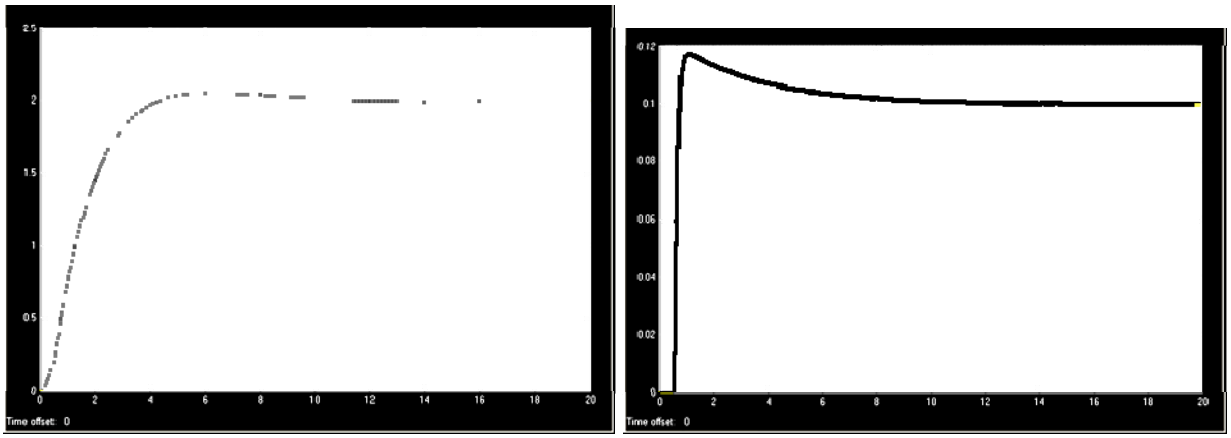

Figure 43: The PID controllers successfully commanded the quad-rotor to achieve the desired altitude and roll angle of 2 m and 0.1 radians, respectively. The Z position is shown on the left, with roll angle on the right.

Though these gains and controllers proved to work in simulation, the controls group performed a more detailed stability analysis on the current model of the system.

6.4 Stability Analysis of Simulated PID Controller

Stability analysis with MATLAB proved to be rather simple with the transfer functions already computed. The stability of a system with a controller can be determined by examining the frequency-response of that system. According to Ogata [13], a useful way of representing the frequency response characteristics of dynamics systems is by producing a Bode diagram (also known as logarithm plots of frequency response). For more information on Bode diagrams, consult Ogata [13].

From the Bode diagram, the phase and gain margins of the system can be determined. The phase margin of a system is an indicator of the amount a system will oscillate due to some step response. Larger phase margins are indicative of systems that are more stable when faced with step inputs. The gain margin indicates how much the gain of a system can be changed before a system becomes unstable. For a minimum-phase system to be considered stable, both the gain and phase margins must be positive; thus, negative margins indicate an unstable system [13]. Typically for a stable, robust control system the phase (Pm) and gain (Gm) margins should be $+30° \leq Pm \leq +60°$ and $Gm > 6$ dB.

Examining the quad rotor system with the control algorithms in Figure 42 and the gains in Table 18, MATLAB was used to create the following Bode diagrams:

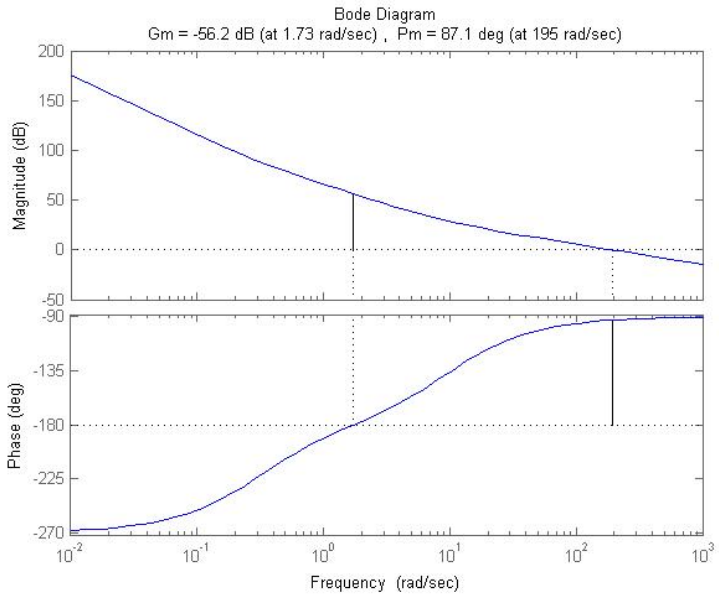

Figure 44: Roll Bode Diagram with -56.2 dB gain margin and 87.1° phase margin

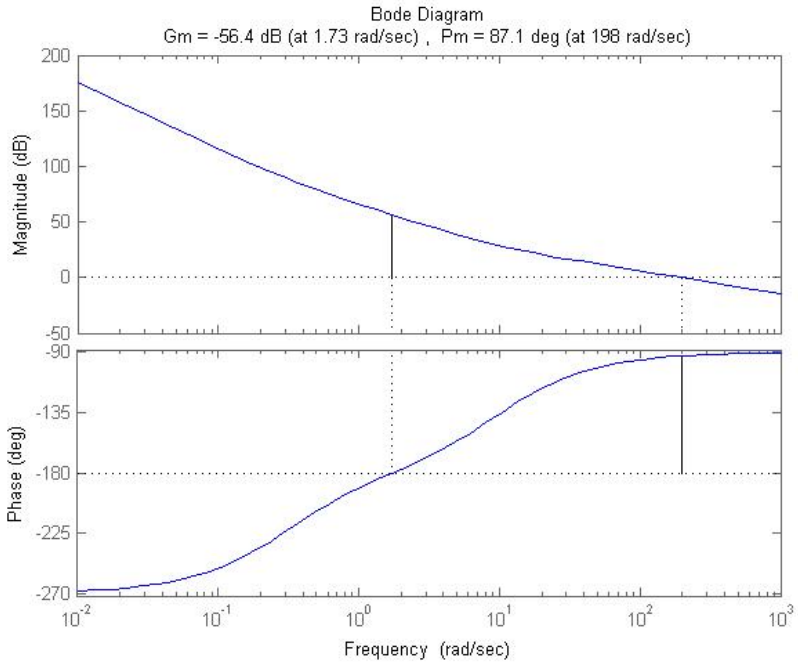

Figure 45: Pitch Bode Diagram with -56.4 dB gain margin and 87.1° phase margin

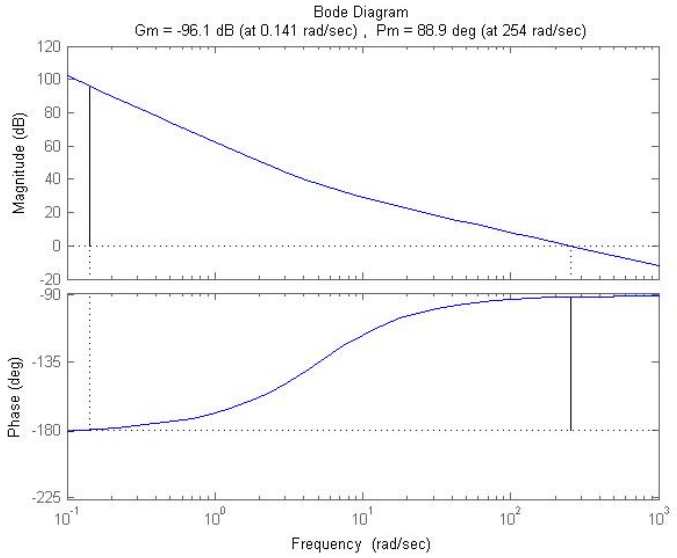

Figure 46: Yaw Bode Diagram with -96.1 dB gain margin and 88.9° phase margin

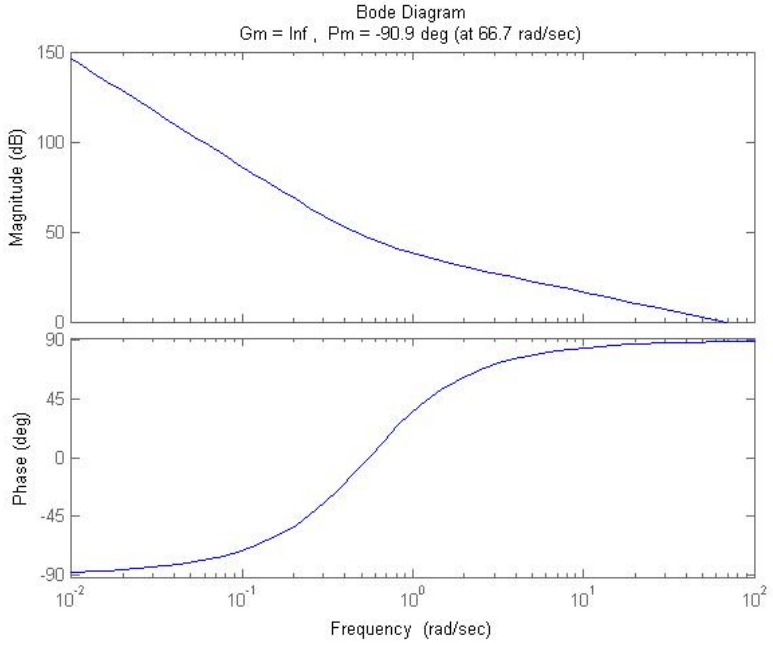

Figure 47: Altitude Bode Diagram with ∞ dB gain margin and -90.9° phase margin

For the attitude controllers (roll, pitch, yaw), all the phase margins were positive; however, the gain margins were all negative in Figure 44, Figure 45, and Figure 46. This indicates that even though the Simulink simulation suggested the system could be commanded and stabilized by the attitude controllers, the real operation of these controllers would lead to an unstable system. The system would resist oscillation due to step input very well because of the

high phase margins; however, any significant error in the gains of the system would lead to system divergence in attitude.

For the altitude controller, the gain margin was infinity, and the phase margin was -90.9° therefore, the system with the current altitude controller would also be unstable. Though the gain in the altitude controller could be changed substantially by any amount, the system would be susceptible to heavy oscillation in altitude with a step input. For example, if the quad rotor was commanded from a zero altitude to a relatively high altitude such as 10 m, the quad rotor would greatly overshoot the desired altitude, undershoot it, and the it would oscillate, possibly never actually reaching 10 m.

The results of this stability analysis indicate that the gains for altitude controller must be lowered substantially because the negative gain margin is analogous to how much it must be decreased to make the system stable [13]. Thus, the controller gains were decreased as a result of these initial simulations.

Also as a recommendation for future works, the altitude controller could be redesigned to control the altitude rate. By controlling the altitude rate, the rate of change of altitude can be decreased and eventually zeroed out at the commanded altitude—separate logic would be needed to determine the desired altitude rate for a given altitude. The effects of controlling the altitude rate are analogous to the increased stability advantages of the derivative controller.

While simulating and tuning the PID controllers, the controls team also examined the hardware that would implement these control algorithms.

6.5 Controls hardware

This section briefly outlines the hardware utilized to implement the controller designed by the controls team. Discussion about the controls hardware will include the sensors needed to measure the state of the quadrotor and the computer needed to implement the control logic.

6.5.1 Microcontroller

The microcontroller is a device that contains an integrated microprocessor, RAM, ROM, and I/O ports. Operating according the program located in the ROM, the microcontroller takes sensor data, interprets these readings, determines an appropriate course of action, and controls the motors through the ESCs to execute this action. In order to receive power, receive data, and control the ESCs, the microcontroller must be integrated with a circuit board.

There are several options available for programming the flight controller, including C/C++, Simulink, and LabVIEW. LabVIEW is the optimum choice since models are easier to put together than in C/C++, the Plantation Road laboratory is licensed to use the LabVIEW Embedded Module for microcontrollers, the lab has experience in using LabVIEW Embedded, and the cost to obtain a license for Simulink for microcontrollers is too great. LabVIEW Embedded permits a user to design a model in LabVIEW, and then compile it for use on a microcontroller, simplifying development and implementation. The primary selection constraint for the microcontroller is that the microprocessor must be compatible with LabVIEW embedded. Other important considerations when selecting a microcontroller include the processing speed, memory, power consumption, and compatibility with the sensors.

The controls team decided to utilize a COTS single board computer to save time and cost. The Robostix board is based around an ATmega128 MCU with 8-Bit Integer Processor running at 16MHz with about16 MIPS,6 Pulse-width modulation (PWM) outputs 8 ADC inputs, 2 UART Input/Outputs, I2C, SPI, and GPIO.

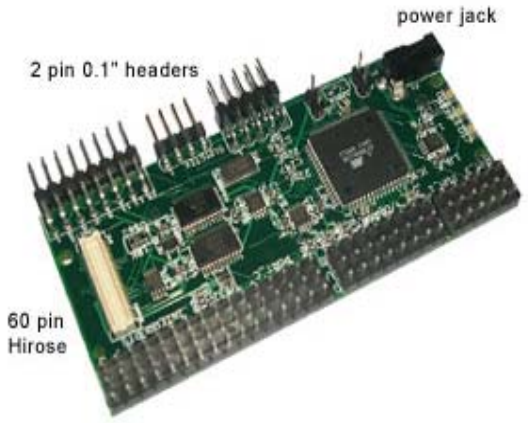

Figure 48: Example of Robostix Controller Board

6.5.2 Inertial Measurement Unit

The inertial measurement unit (IMU) is a sensor that uses accelerometers and gyroscopes to detect acceleration and angular rate. A typical IMU utilizes a triaxial accelerometer and triaxial gyro to obtain motion information over six degrees of freedom. From these rates, it is possible to calculate the velocity, position, and heading. However, error from the sensors will accumulate over time, resulting in 'drift' or incorrect position and attitude determination. Other methods must be used in order to ensure the calculated position and attitude is correct.

An IMU may also contain temperature sensors for data correction since the accelerometer and gyro readings are thermally sensitive. Some IMUs also include magnetometers to assist in heading determination by using the surrounding magnetic field as a reference. This reading is not subject to drift over time in a steady magnetic field, but is sensitive to magnetic field variations that would typically be encountered indoors.

While the resources are available to construct the IMU in-house, the lack of experience and time required to do so make this option unfeasible. Instead, a commercial-of-the-shelf (COTS) IMU will be used. Several COTS IMUs were examined in a trade study, with a serial interface, accelerometer and attitude outputs as the highest priorities. Other important factors are error detection and correction, weight, power use, and cost. The results of the trade study are shown in Table 19.

Table 19: Inertial Measurement Unit decision matrix. [14]

Specification	Weighting	Microstain 3DM-GX2	Microstrain 3DM-GX1	Memsense nIMU	Memsense uIMU
Serial Interface	15	1	1	1	1
Sensor Misalignment Detection	7.5	1	1	1	1
Temperature Bias Detection	7.5	1	1	1	1
Gyro G-Force Influence Detection	7.5	1	1	0	0
Accelerometer Output	15	1	1	1	1
Attitude Euler Angle Output	10	1	1	0	0
Attitude Angle Rate Output	5	0	0	1	1
Weight	10	1	0	0	-1
Power Consumption	7.5	1	1	-1	-1
Data Refresh Rate	5	1	0	-1	-1
Cost	10	0	1	1	-1
Total	**100**	**85**	**80**	**47.5**	**17.5**

The Microstrain 3DM-GX2, shown in Figure 49: The Microstrain 3DM-GX2 IMU.Figure 49, is the IMU that best fits the mission requirements. This unit also includes an on-board processor that interprets the sensor readings and outputs data.

Figure 49: The Microstrain 3DM-GX2 IMU. [15]

6.5.3 Rangefinders

The quadrotor must be able to navigate autonomously within a building, move through hallways and doorways, and avoid obstacles such as furniture in order to locate the control panel described by the IARC rules. To do this, it is necessary that the quadrotor be aware of its surroundings. Infrared and ultrasonic rangefinders are to be used to determine the distance to obstacles. The data these sensors obtain are to be utilized by the microcontroller as part of the navigation program. The rangefinder readings may also be used to correct for drift from accumulated error for the position and attitude determinations derived from the IMU. These sensors were selected due to low cost, weight, and power usage, as well as past successful use in other autonomous systems.

6.5.3.1 Infrared sensor

The infrared rangefinder, as shown in Figure 50, is a small, low-cost device that operates using triangulation. An emitter gives off a pulse of an infrared light. This light then reflects off an obstacle and back to a sensor next to the emitter. The sensor is a linear CCD array, and this measures the reflected beam angle. From this angle, the distance to the obstacle can be determined.

The IR sensor has a short functional range of about a meter, depending on the selection. The sensor is sensitive to sources of IR light, such as incandescent light and sunlight. The IR beam is also relatively narrow, which is optimal for longer distance ranging of large surfaces or walls, but may miss thinner obstacles like chairs.

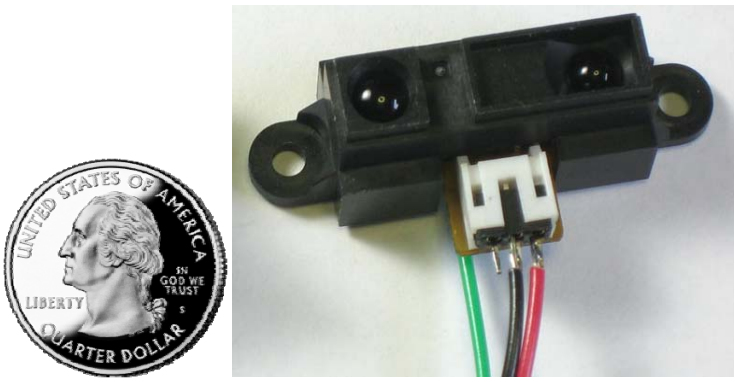

Figure 50: Infrared rangefinder sensor. [16]

These sensors were previously used on an AAVT robotics project called the Micromouse (Figure 51). Using three IR sensors, the Micromouse was able to navigate around a room by following the walls. The navigation programming from the Micromouse is to be adapted for use with the quadrotor.

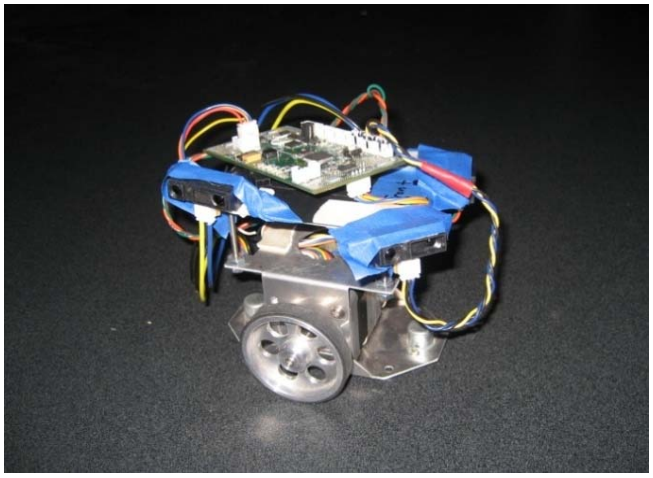

Figure 51: The AAVT Micromouse robot. [14]

6.5.3.2 Ultrasonic sensor

The ultrasonic sensor is an inexpensive rangefinder that utilizes high-frequency sound to determine the distance to an obstacle. The device emits a sound pulse and measures the time to echo, and the distance can be determined using this and the speed of sound. This sensor is small, has a longer range than the IR sensor, and has a finer resolution that permits it to sense smaller objects. This sensor will be used primarily as an altimeter, and will be aimed at the floor. There is a possibility that the sound that the quadrotor generates may interfere with the sensor readings, so this issue will be examined in the future.

The final selection of the ultrasonic sensor is not yet complete, however the Maxbotix LV-MaxSonar-EZ4 is a likely choice. The EZ4 has a 6.45 meter range, maximum 20Hz reading rate, and serial output.

Figure 52: LV-MaxSonar-EZ4 rangefinder.[17]

6.5.4 Standing

C programming language was used to program the microcontroller, and the microcontroller was selected to be the Robostix board. The quadrotor will use a Microstrain IMU and rangefinders as part of the navigation. Infrared and ultrasonic rangefinders would be used for obstacle detection.

6.6 Controlling the System in Reality

6.6.1 Scope

Simulink and Labview are great software packages for simulating dynamics and controls; however, the reality of controlling a quadrotor system is much more complex. Reality brings random error into a dynamic system; thus, the controller must be designed so that it is robust enough to handle this uncertainty and dynamically stabilize the system in the presence of high perturbations [18]. To accurately develop the controller, the controls team used the altitude, 1-DOF (one degree of freedom), and yaw test stands constructed by the propulsions team.

6.6.2 Hardware/Software Integration

The controls team used AVR Studio to compile the C-code of the controller. This program was used in conjunction with an AVR chip programmer to load the controller code onto the Robostix controller. The Robostix board communicates with the speed controllers via pulse-width modulation (PWM) signal. As part of a simple hardware integration test, the controls team tested the throttle control of the Robostix.

A Dell Latitude laptop computer sent throttle commands to the AVR chip programmer that relayed the command to the Robostix board. Five commands were tested—0%, 25%, 50%, 75%, and 100% throttle. Once the command was sent to the Robostix board, it was echoed via

serial cable back to the computer to confirm that the command was received. Simultaneously, the Robostix commanded the speed controllers to the desired throttle. The controls team used this simple testing to confirm the integrity of all wire connections as well as the ability of the Robostix to command throttle to the speed controllers (and thus the motors).

6.6.3 Altitude Testing

Once the was tested and working properly, the controls team tested its PID altitude controller with the quad rotor on the altitude test stand. Altitude was measured using an infrared distance sensor mounted on the underside of one of the motor spars. The infrared sensors measured the altitude in the way discussed in the previous control hardware section. Hardware for this test included the Robostix board, the AVR Chip Programmer, one laptop computer with serial connection, and the quad rotor fully equipped sans mission sensors and mission computer. The computer commanded the altitude via the programmer. The altitude commands flowed on the user-to-computer, computer-to-programmer, programmer-to-robostix, robostix-to-speed controller, and speed controller-to-motor data stream. The altitude command flow is shown below in Figure 53.

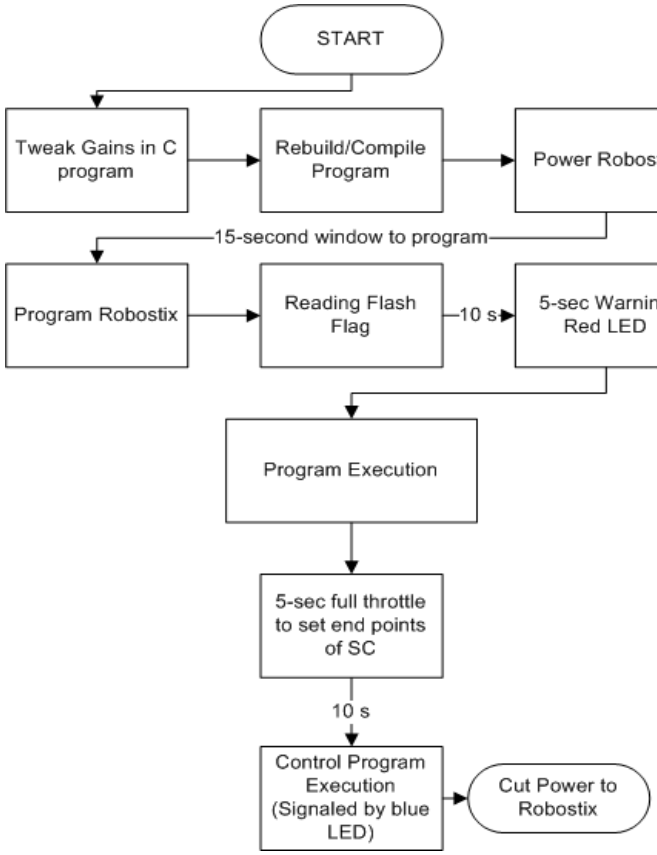

Figure 53: Altitude Testing Procedure

Initially, the altitude controller was a PID controller with a low-pass filter on the altitude state, which means that the controller would filter out any frequency above the cutoff frequency, and thus reduce the amplitude of the command. This was done to ensure that errors in the altitude measurement would not drive the controller to increase altitude so rapidly that the vehicle would impact the cutoff block of the test stand (or fly beyond that point and crash). The flowchart in Figure 53 demonstrates the test procedure accurately. For safety purposes, testers wore safety glasses and hands were kept clear of the prop plane while the propellers were active.

The derivative gain was set higher than the proportional gain to increase damping of the system. Initial tests with lower derivative gain yielded highly unsteady system dynamics; the quadrotor would not stabilize at the desired altitude, which was about 12 inches above the bottom of the altitude test stand. Including an integral term also increased oscillation in the system, which was preventing the controller from damping out errors in the altitude state. The proportional term was scaled to be about 40-60% of the derivative term. This gain arrangement led to a PD controller that damped out large oscillations and stabilized the system to a desired altitude.

This gain tuning and test procedure resulted in the elimination of the integral term of the controller; thus, the resulting controller for the dynamic system was a PD (Proportional-Derivative) controller. The controls team deemed that the quad rotor system lacked clear steady-state error that would require a non-zero integral gain term (K_i). The PD controller proved sufficient in providing artificial damping and relatively agile command response. No controller response data versus commanded altitude exists because the data was not passed back to the computer during testing.

6.6.4 Pitch/Roll/Yaw Testing

Since the controller is comprised of multiple SISO controllers and the vehicle was designed to be approximately symmetric about both the pitch and roll axes, pitch and roll control testing were completed on the 1-DOF test stand constructed by the propulsion team (See Section 5.11, Figure 34). Presently, the PD controller was copied from the altitude algorithm and the gains were changed accordingly to control the pitch/roll. The controls team initially experienced an extreme overshoot in commanded pitch/roll on the test stand which lead to a divergence in stability. Instead of asymptotically stabilizing to the commanded angle over time, the system would oscillate more violently with time. The gains were adjusted and eventually the controllers

commanded the quadrotor to the desired pitch and roll angles. The pitch and roll controllers were also tested in tethered flight as shown in Figure 54.

Figure 54: Tethered Pitch/Roll Testing

During this tethered testing, the controllers attempted to command the pitch and roll angles in the presence of gusts (which are considered a high perturbations). After hit by a large gust of wind, the quadrotor began to wobble about its yaw axis. The intermediate axis of the quadrotor is located somewhere between the pitch and roll axes. Furthermore, the quadrotor was rotating about the intermediate axis during the tethered test. Due to energy dissipation, a stable rotation about the intermediate axis is not possible, so eventually the system will start to rotate about its major axis. This was exactly the case for the quadrotor in the tethered test. The wobble was induced by the quadrotor system trying to rotate about its yaw axis—the major axis. There was no yaw control implemented during this test, so in the future, this test will need to be repeated with yaw control to demonstrate that yaw control will eliminate the wobble.

Yaw testing was completed by utilizing the yaw test stand shown in Figure 35 of Section 5.12. After sufficient gain tuning, the quadrotor was easily controlled even in the presence of pertubations; any desired heading could be achieved. An example of inducing perturbations during the yaw testing is shown in Figure 55.

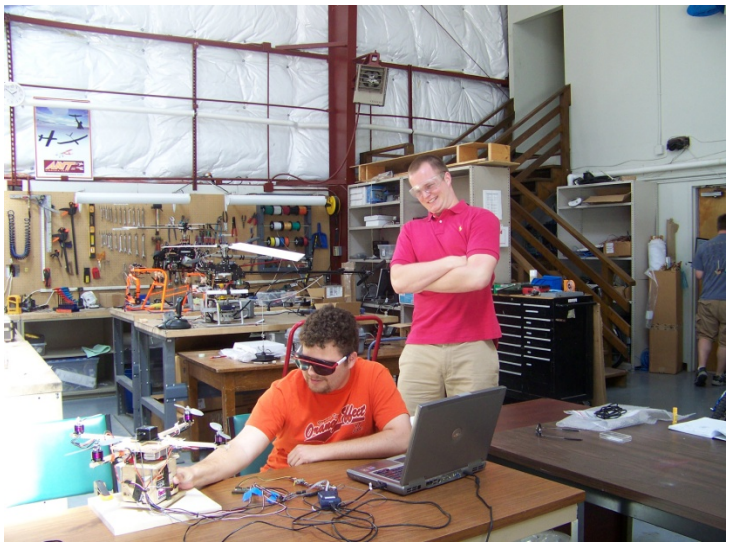

Figure 55: Yaw Controller Testing on Yaw Test Stand

No controller response data versus commanded pitch, roll, or yaw exists because the data was not passed back to the computer during testing.

6.6.5 Testing Results

After completion of the altitude and attitude testing, gains were determined for each SISO controller as shown in Table 20.

Table 20: Control Gains

SISO Controller	K_p (Proportional)	K_d (Derivative)
Altitude	1.5	-5
Roll/Pitch	15	2.75
Yaw	-20	3

The controls team determined that there was a lack of steady-state error in the quadrotor system; thus, the integral term in the controller was unnecessary. Also, the optimal controller frequency (sampling time) was determined to be 20 Hz.

6.7 Path Forward

At this point the controls team is gain tuning the pitch, roll, and yaw controllers so that an untethered flight could be feasible. In the future, other control schemes should be investigated early in the process, such as output tracking methods, specifically Linear Quadratic (LQ) output

tracking methods. More sophisticated gain tuning methods would also help to reduce trial and error gain tuning that takes an exorbitant amount of time. For example, one can simulate a LQ output tracking controller in Simulink against a nonlinear dynamics model. Integral-Backstepping control methods were also popular among academia in dissertations and theses.

Early simulations done by the controls team used a linear approximation when examining the system response, which yields uncharacteristically good tracking to commanded values. Work has been done to implement a nonlinear model in Simulink; however, logic to simulate the rotor dynamics, system lag, or white noise has not been included in the simulation. With a relatively accurate simulation, a controller can be tuned fairly well before actual testing ever occurs. Once a robust controller is tuned and it successfully controls the quadrotor after multiple tests, un-tethered flight tests are the next logical step. Work will be done on the controller until the very end of the academic year.

7.0 Status and Recommendations

This section will include the current status of the Weights and Structures, Propulsion, and Controls groups respectively. Recommendations for future teams will also be presented.

7.1 Weights and Structures

The structures team has accomplished most goals set this year in building a viable quadrotor design, though a few tasks still remain. The structures team has created designs for and built the Proto1 test bed quad rotor. The design for Proto2 has been finalized, with all but the shrouds having been fabricated. Once attached along with the motors and electronics of the propulsion and controls teams, the structures team will have accomplished its objectives.

It is recommended that any additional work in the future begin with optimizing some of the components on Proto2. While the Proto2 design meets all objectives as a light weight quadrotor, some features, specifically the shrouds, could possibly be redesigned to be stronger, simpler and lighter. Additionally, at the current time there had not been any confirmation from the ME sensors team on what the specific layout and dimensions of the payload would need to be. As such, future structures work could be done on helping design and build the payload box if given the needed parameters.

7.2 Propulsion

The Propulsion Team has accomplished all objectives set this year to develop a propulsion system satisfying the requirements of this competition and to implement it on the first prototype. The components of the second system have been ordered and will be implemented on Proto2 when they arrive. The team has also created several test stands to be used by the controls group to aid in the development of the flight controls for the vehicle. For the remainder of the duration of the project, the Propulsion team will be tasked with maintaining and (whenever necessary) replacing parts of the propulsion system.

A future Propulsion Team might be tasked with the job of creating improved test stands whose effects on the system dynamics are well known. The team might also continue research in improvements of motor, propeller, ESC or battery technology that might improve on the performance of the current propulsion system.

7.3 Controls

To date, the control algorithm is comprised of four, independent SISO controllers that are able to command the quadrotor to a desired attitude and altitude in the absence of large

perturbations. This is a concern that needs to be addressed by future teams. Though the competition would be indoors, buildings still possess air ducts that can induce heavy gusts. Plus, the quadrotor will likely impact walls during the mission, which will introduce more perturbations into the system. It is recommended that a more robust controller, such as an LQ ouput tracker or Integral Backstepping algorithm, be explored and utilized.

Free, untethered flight has not yet been achieved by the controls team. Before this milestone can be reached, testing of the translational dynamics of the quadrotor during flight will be crucial. Future teams will need to simulate and test the flight dynamics, most likely with Simulink and IMU-assisted, RC-controlled flight. It is recommended that the dynamics be simulated with a non-linear dynamics model; the results will be more accurate. The nonlinear model will also be useful to more accurately tune the controller before hardware testing takes place.

The quadrotor vehicle was not arranged in a mission configuration during controls testing; the Robostix board was not mounted on the vehicle and the mission payload was not complete. The controls team is concerned with this for several reasons; the effects of electromagnetic interference between hardware components was not examined, and hardware resilience was not tested either. Future teams should investigate the effects of electromagnetic interference on hardware performance, specifically between the motors, Robostix board, and sensors. The next teams will also need to secure and protect valuable hardware before attempting free, untethered flight by designing a collision absorber of some kind.

Once future teams complete the design of a robust controller, it will need to be integrated with the outer-loop navigation algorithm. To date, the navigation algorithm has not been designed. With a robust navigation and control algorithms, it will be possible to achieve stable, untethered, controlled flight with the quadrotor vehicle.

8.0 Acknowledgements

The Aerospace IARC team would like to thank Ryan Ilardo for all his help he provided during his free time for design suggestions and CNC machine usage. The authors would like to thank Aaron Oberste of the ME controls team for his expertise and hardware savvy. The Aerospace IARC Controls team also owes a debt of gratitude to Chris Cotting for his help in teaching advanced controls. Without Chris's help, the Aerospace controls team would not have possessed enough knowledge to command the quadrotor to steady attitude and altitude.

9.0 References

[1] Rules for the International Aerial Robotics Competition 5th Mission. [Online] [Cited: December 11, 2008.] http://iarc.angel-strike.com/IARC_5th_Mission_Rules.pdf.

[2] "BYU Quad Rotor Senior Project.". *Brigham Young University.* [Online] [Cited: December 11, 2008.] http://www.et.byu.edu/groups/quad08buldog/structure/basic_design.php.

[3] UAV Laboratory. *Clemson Univerisity.* [Online] ECE Department. [Cited: December 11, 2008.] http://www.ece.clemson.edu/crb/research/uav/index.htm.

[4] **Beer, Ferdinand P., Johnston, E. Russel and DeWolf, John T.** *Mechanics of Materials.* New York, NY : s.n., 2006.

[5] Automation Creations, Inc. *MatWeb.com.* [Online] [Cited: December 11, 2008.] http://www.matweb.com/.

[6] Power Systems. *RCGroups.* [Online] 2004. http://www.rcgroups.com/forums/showthread.php?t=232300.

[7] A10 Series Motors. *Hackerbrushless.* [Online] 2008. http://www.hackerbrushless.com/motordetails.aspx?series=a10.

[8] A20 Series Motors. *Hackerbrushless.* [Online] 2008. http://www.hackerbrushless.com/motordetails.aspx?series=a20.

[9] Phoenix-10 Brushless Motor Control. *Castle Creations.* [Online] 2006. http://www.castlecreations.com/products/phoenix-10.html.

[10] Phoenix-25 Brushless Motor Control. *Castle Creations.* [Online] 2006. http://www.castlecreations.com/products/phoenix-25.html.

[11] ThunderPower Batteries. *ThunderPower RC.* [Online] http://www.thunderpowerrc.com/html/prolites.html.

[12] ELogger V3. *Eagle Tree Systems.* [Online] 2005. http://www.eagletreesystems.com/micropower/micro.htm.

[13] **Ogata, Katsuhiko.** *System Dynamics: Fourth Edition.* Upper Saddle River, NJ : Prentice Hall, 2004.

[14] **Autonomous Aerial Vehicle Team.** *IARC Final Report.* Blacksburg : s.n., 2008.

[15] **MicroStrain, Inc.** 3DM-GX2 MicroStrain AHRS Orientation Sensor. *MicroStrain.* [Online] [Cited: December 11, 2008.] http://www.microstrain.com/3dm-gx2.aspx.

[16] **Solarbotics Ltd.** I2C-lt IR Rangefinder. *HVW Technologies.* [Online] [Cited: December 11, 2008.] http://www.hvwtech.com/products_view.asp?ProductID=665.

[17] **Maxbotix, Inc.** LV-MaxSonar-EZ4 Datasheer. *Maxbotix.* [Online] [Cited: December 11, 2008.] http://www.maxbotix.com/uploads/LV-MaxSonar-EZ4-Datasheet.pdf.

[18] **Bouabdallah, Samir.** *Design and Control of Quadrotors with Application to Autonomous Flying.* 2007.

[19] **NXP Semiconductors.** LPC23xx Microcontrollers. *NXP Semiconductors.* [Online] [Cited: December 11, 2008.] http://www.standardics.nxp.com/products/lpc2000/lpc23xx/.

10.0 Appendix

Appendix A – IARC Budget and Parts List

Budget	**$1,650.00**
Total Spent	**$2,575.04**
Budget Balance	**($925.04)**

New Budget	***$3,000.00***
New Budget Balance	***$424.96***

IARC BUDGET AND PARTS LIST

Part Name	*Manufacturer*	*Part Number*	*Unit Price*	*QTY*	*Total Price*	*Purchase Date*	*Retail Host*
Top Flite Power Point Balancer	Tower Hobbies	LXHY61	$19.99	1	$19.99	16-Oct-08	Tower Hobbies
APC 7x4 Propeller	Tower Hobbies	LX1507	$1.69	1	$1.69	16-Oct-08	Tower Hobbies
APC 7x6 prop	Tower Hobbies	LX1509	$1.69	1	$1.69	16-Oct-08	Tower Hobbies
APC 7x8 Prop	Tower Hobbies	LX1511	$1.75	1	$1.75	16-Oct-08	Tower Hobbies
APC 8x4 Prop	Tower Hobbies	LX1517	$1.99	1	$1.99	16-Oct-08	Tower Hobbies
APC 8x6 Prop	Tower Hobbies	LX1519	$1.99	1	$1.99	16-Oct-08	Tower Hobbies
APC 8x8 prop	Tower Hobbies	LX1521	$1.99	1	$1.99	16-Oct-08	Tower Hobbies
APC 9x4 Prop	Tower Hobbies	LX1532	$2.19	1	$2.19	16-Oct-08	Tower Hobbies
APC 9x6 Prop	Tower Hobbies	LX1534	$2.19	1	$2.19	16-Oct-08	Tower Hobbies

Appendix B – IARC Budget Breakdown

IARC BUDGET BREAKDOWN

Department	*Dept. Budget*	*Part Name*	*Unit Price*	*QTY*	*Total Price*
PROPULSION	***$850.00***	Top Flite Power Point Balancer	$19.99	1	$19.99
		APC 7x4 Propeller	$1.69	1	$1.69
	Dept. Balance	APC 7x6 prop	$1.69	1	$1.69
	$812.34	APC 7x8 Prop	$1.75	1	$1.75
		APC 8x4 Prop	$1.99	1	$1.99
	New Budget	APC 8x6 Prop	$1.99	1	$1.99
	$2,400.00	APC 8x8 prop	$1.99	1	$1.99
		APC 9x4 Prop	$2.19	1	$2.19
	New Dept. Bal.	APC 9x6 Prop	$2.19	1	$2.19
	$2,362.34	APC 9x8 Prop	$2.19	1	$2.19
					Total Cost $37.66

Department	*Dept. Budget*	*Part Name*	*Unit Price*	*QTY*	*Total Price*
STRUCTURE	$300.00	1/4" x 6" x 2' Choice Maple	$3.39	1	$3.39
		3/8 x 3/8 x 24 Basswood	$1.19	2	$2.38
	Dept. Balance	Misc Nuts, Bolts, Screws, Etc.	$0.11	16	$1.76
	$290.23	Misc Nuts, Bolts, Screws, Etc.	$0.14	16	$2.24
					Total Cost $9.77

Department	*Dept. Budget*	*Part Name*	*Unit Price*	*QTY*	*Total Price*
TOOLS	$300.00	American Weigh AMW-2000 Bench Scale 2000x0.1g	$99.95	1	$99.95
		25W Solderin Iron	$10.99	1	$10.99
	Dept. Balance	.75 OX .050 Elec Solder	$2.99	1	$2.99
	$184.08	45-308 20PAK 8IN Cable Tie	$1.99	1	$1.99
					Total Cost $115.92

PARTS LIST FOR CF PROTOTYPE

Department	***Part Name***	***Unit Wt (g)***	***Unit Price***	***QTY***	***Total Wt (g)***	***Total Price***
PROPULSION	ThunderPower Pro Lite 2600 mAh 11.1 V 3 Cell Battery	185.5	$74.99	2	371	$149.98
	Hacker A20-30M Brushless Outrunner Motor	53.7	$54.99	4	214.8	$219.96
	Castle Creations Phoenix 25 ESC	17.4	$57.99	4	69.6	$231.96
	Battery Y-Harness	16.2	$7.10	2	32.4	$14.20
	Hobbico Pro HD Y-Harness					
	JR/Hitec/Air Z (for ESC)	21.4	$11.99	1	21.4	$11.99
	APC 8x3.8 Slow Flyer Counter Rotating Propellers	7.3	$7.59	4	29.2	$30.36
	Receiver	40.3	$0.00	1	40.3	$0.00
					Total Wt. (g)	***Total Cost***
					778.7	***$658.45***

Department	***Part Name***	***Unit Wt (g)***	***Unit Price***	***QTY***	***Total Wt (g)***	***Total Price***
STRUCTURE						
					Total Wt. (g)	***Total Cost***
					0	***$0.00***

Department	***Part Name***	***Unit Wt (kg)***	***Unit Price***	***QTY***	***Total Wt (kg)***	***Total Price***
CONTROLS	ME PAYLOAD	N/A	N/A	1	N/A	N/A
					Total Wt. (kg)	***Total Cost***
					0	***$0.00***
					PROTO WT. (kg)	***PROTO COST***
					778.7	***$658.45***

```
%
N0040 G0 G90 X1.6999 Y1.5113 S0 M03
N0050 G43 Z.1181 H00
N0060 G1 Z-.05 F9.8 M08
N0070 G0 Z.1181
N0080 G1 Z-.0008 F4.9
N0090 Z-.1 F9.8
N0100 G0 Z.1181
N0110 G1 Z-.0508 F4.9
N0120 Z-.15 F9.8
N0130 G0 Z.1181
N0140 G1 Z-.1008 F4.9
N0150 Z-.2 F9.8
N0160 G0 Z.1181
N0170 G1 Z-.1508 F4.9
N0180 Z-.2226 F9.8
N0190 G0 Z.1181
N0200 M02
%
```

Figure 56: Sample partial G-code used to create motor mount base on CNC machine